



**Improved Nuclear Site characterization for waste minimization  
in DD operations under constrained Environment**

Research and Innovation action  
NFRP-2016-2017-1

# **Statistical approach guide - UC3a Annex - Deliverable D3.7**

Version n° 1

**Authors: Y. Desnoyers (Geovariances), N. Pérot (CEA)**

**<http://insider-h2020.eu/>**



*This project has received funding from the Euratom research and training programme 2014-2018 under the grant agreement n°755554 .  
The content in this deliverable reflects only the author(s)'s views. The European Commission is not responsible for any use that may be made of the information it contains.*



## Document Information

Grant Agreement #: 755554

Project Title: Improved Nuclear Site characterization for waste minimization in DD operations under constrained Environment

Project Acronym: INSIDER

Project Start Date: 01 June 2017

Related work package: WP 3: Sampling strategy

Related task(s):

Lead Organisation: Geovariances

Submission date:

Dissemination Level: Confidential

## History

Date	Submitted by	Reviewed by	Version (Notes)

## Table of contents

List of Tables .....	3
List of Figures .....	3
Summary .....	6
<b>1 Annex 3: UC3a Summary .....</b>	<b>7</b>
<b>1.1 Overall strategy.....</b>	<b>7</b>
1.1.1 Request for initial characterization .....	7
1.1.2 Define objectives .....	7
1.1.3 Gather pre-existing records/data .....	8
1.1.4 Is data sufficient for analysis? .....	11
1.1.5 Can more samples be collected?.....	12
<b>1.2 Data analysis &amp; sampling design .....</b>	<b>13</b>
1.2.1 Pre-processing and exploratory data analysis.....	13
1.2.2 Data analysis and modelling.....	17
1.2.3 Post-processing with geostatistics model variants and subsampling variants.....	26
1.2.4 Post-processing with limits of detection and measurement uncertainties treatment.....	36
<b>1.3 Is the objective achieved?.....</b>	<b>46</b>
1.3.1 Estimate and uncertainty impact synthesis.....	46
1.3.2 Overall conclusions and sampling recommendations.....	47

## List of Tables

Table 1: Proportion of valid data and LOD for each radionuclide and each plan H1 (-0.5m) and H2 (-1.5m). .....	13
Table 2: Synthesis of geostatistics model variants and subsampling variants. ....	25
Table 3: Normality statistical test analysis on valid data. ....	26
Table 4: Total activity for the three main nuclides (GBq) for the reference case and for levels H1 (-0.5m) and H2 (-1.5m).....	27
Table 5: Robustness and indicators of prediction quality for the different methods performed on the three studied radionuclides. ....	37
Table 6: Mean and median estimation of total activity with the empirical approach (circles).....	37
Table 7: Median and 5% and 95% quantile estimates of total activity for the three studied radionuclides and both levels. ....	44
Table 8: Sensitivity analysis on results (both estimate and related uncertainty). ....	47

## List of Figures

Figure 1: Vertical cross section of the two horizontal drilling layers. ....	8
Figure 2: Top view of the angular distribution of drill holes. ....	9
Figure 3: Sonic drilling machine similar to the one used on UC3.....	9
Figure 4: Different steps for drilling samples. ....	10
Figure 5: Raw drilling core (top) and result of size segregation (bottom). ....	11
Figure 6: Base maps of the two sampled layers, H1 on left with boreholes A, B and C, H2 on the right with boreholes D, E, F and G. ....	11
Figure 7: Base maps of gamma scanning for level H1 at -0.5m (left) and H2 at -1.5m (right). No gamma scanning was performed on borehole G.....	12

Figure 8: Histograms of the three nuclides (Bq/kg). In blue: data below quantification limit. ....	14
Figure 9: Histograms for the uncertainties of the three main radionuclides.....	15
Figure 10 : Correlation (log scale) between measurement and related uncertainty for the three nuclides (Bq/kg). Identification of outliers. Colorscale related to borehole ID.....	16
Figure 11: Linear correlation coefficients between radionuclides A, B and C.....	17
Figure 12 : Gaussian anamorphosis of log10 transformed data for nuclide A. This bijection between real distribution (Y axis) and corresponding Gaussian transformation (X axis) enables more advanced geostatistical analysis and results.....	18
Figure 13 : Multivariate (nuclides A, B and C) experimental variograms with two horizontal directions and vertical. Top right base map explains orientation in the horizontal plane. The 3 simple variograms are on the diagonal and the 3 cross-variograms in the bottom left part.....	19
Figure 14 : Fitted multivariate omnidirectional variogram. Dashed line on cross-variograms represents the maximum correlation envelope.....	20
Figure 15: Model structures and sills for multivariate reference case. ....	21
Figure 16 : Model structures and sills for the case integrating a 15% nugget effect.....	21
Figure 17 : Model structures and sills for the multivariate case with Gamma scanning.....	22
Figure 18 : 2m subsampling variants #1/2 (left) and #2/2 (right). Black circles are removed data points. Colorscale for nuclide C (Bq/kg). ....	23
Figure 19: 4m subsampling variants #1/4, #2/4, #3/4 and #4/4. H1 (-0.5m) on the upper part, H2 (-1.5m) on the lower part. Black circles are removed data points. Colorscale for nuclide C (Bq/kg). ....	24
Figure 20: Mean of 500 simulations for Nuclide C (Bq/kg). Left: H1 (-0.5m); right: H2 (-1.5m). ....	27
Figure 21: Standard deviation of 500 simulations for Nuclide C (Bq/kg). Left: H1 (-0.5m); right: H2 (-1.5m). ....	27
Figure 22: Total activity for nuclide C (GBq), levels H1 at -0.5m (left) and H2 at -1.5m (right) depending on the variant.....	29
Figure 23: Median and 90% confidence interval for nuclide C total activity depending on the variant, Level H1 (-0.5m). ....	29
Figure 24: Median and 90% confidence interval for nuclide C total activity depending on the variant, Level H2 (-1.5m). ....	30
Figure 25 : Raw and logarithmic histograms for nuclide C showing values inferior to QL in blue...	31
Figure 26: Evolution of remediation volumes linked to nuclide C contamination depending on the threshold and for different risks (quantiles), Level H1 (-0.5m). ....	31
Figure 27: Evolution of remediation volumes linked to nuclide C contamination depending on the threshold and for different risks (quantiles), Level H2 (-1.5m). ....	32
Figure 28: Remediation volumes for IRAS threshold depending on the variant, levels H1 at -0.5m (left) and H2 at -1.5m (right).....	33
Figure 29: Remediation volumes for IRAS threshold depending on the variant and for different risks (quantiles Q10 – Q30 – Q50), Level H1 at -0.5m. ....	33
Figure 30: Remediation volumes for IRAS threshold depending on the variant and for different risks (quantiles Q10 – Q30 – Q50), Level H2 at -1.5m. ....	34
Figure 31: Comparison of probability that $IRAS \geq 1$ for the reference case (left) and with a nugget effect (right).....	35
Figure 32: Comparison of probability that $IRAS \geq 1$ for 2 possible 4m-subsampling using Gamma scanning or not. ....	35
Figure 33: Evolution of remediation volumes depending on the IRAS threshold for the Reference Case and considering quantile 30%. First bisector line in green.....	36
Figure 34: Strategy to calculate an empirical median estimation of total activity.....	37



Figure 35: Spherical model variogram fitted for *Geo* method on left (a) and for *Geo+LOD+U* method on right (b) for  $\log(\text{Activity})$  of nuclide B at level -0.5m (H1)..... 38

Figure 36: Residual analysis representation for *Geo* method on left (a) and for *Geo+LOD+U* method on right (b) for  $\log(\text{Activity})$  of nuclide B at level -0.5m (H1)..... 38

Figure 37: Cross validation scatter plot for *Geo* method on left (a) and *Geo+LOD+U* method on right (b) on lognormal transformation of nuclide B activity at level -0.5m (H1). ..... 39

Figure 38: Estimation cartography of  $\log_{10}(\text{activity})$  for nuclide B provided with ordinary kriging on data without uncertainty and specific treatment for limits of detection (*Geo*) on the left (a), with uncertainty and specific treatment for limits of detection with *Geo+LOD+U* method in the middle (b) at level -0.5m (H1). ..... 39

Figure 39: Cartography representation of difference between *Geo* ordinary kriging predictions and *GEO+LOD+U* ordinary kriging predictions for activity of nuclide B at level -0.5m (H1). ..... 39

Figure 40: Kriging variance for *Geo* method on left (a) and for *Geo+LOD+U* method on right (b) for  $\log_{10}(\text{nuclide B})$  at level -0.5m (H1). ..... 40

Figure 41: Quantile curve estimations and median estimation cartography of  $\log_{10}(\text{activity})$  for nuclide B provided with *PM+LOD+U* method at level H1 (-0.5m). ..... 40

Figure 42: Spherical model variogram fitted for *Geo* method on left (a) and for *Geo+LOD+U* method on right (b) for nuclide B at level H2 (-1.5m)..... 41

Figure 43: Residual analysis representation for *Geo* method on left (a) and for *Geo+LOD+U* method on right (b) for  $\log(\text{nuclide B})$  at level H2 (-1.5m)..... 41

Figure 44: Cross validation scatter plot for *Geo* method on left (a) and *Geo+LOD+U* method on right (b) on lognormal transformation of nuclide B activity at level H2 (-1.5m). ..... 42

Figure 45: Estimation cartography of  $\log_{10}(\text{activity})$  for nuclide B provided with ordinary kriging on data without uncertainty and specific treatment for limits of detection *with Geo* on left (a) and with uncertainty and specific treatment for limits of detection with *Geo+LOD+U* method on right (b) at level H2 (-1.5m). ..... 42

Figure 46: Cartography representation of difference between *Geo* ordinary kriging predictions and *GEO+LOD+U* ordinary kriging predictions for activity of nuclide B at level H2 (-1.5m). ..... 42

Figure 47: Kriging variance for *Geo* method on left (a) and for *Geo+LOD+U* method on right (b) for  $\log_{10}(\text{nuclide B})$  at level H2 (-1.5m). ..... 43

Figure 48: Quantile curve estimations and median estimation cartography of  $\log(\text{activity})$  for  $\log_{10}(\text{Nuclide B})$  provided with *PM+LOD+U* method at level H2 (-1.5m). ..... 43

Figure 49: Convex hull of data measurements used for geostatistical simulations at level H1 (-0.5m) on left and level H2 (-1.5m) on right. .... 43

Figure 50: Median estimations from simulations the three nuclide total activity for the three methods and empirical estimation for H1 plan (level H1 at -0.5 m). ..... 44

Figure 51: Median estimations from simulations of the three nuclide total activity for the three methods and empirical estimation for H2 plan (level H2 at -1.5 m)..... 44

Figure 52: Quantile estimations of total activity for the three methods for H1 plan (level -0.5 m) on left (a) and H2 plan (level -1.5 m) on right (b). ..... 45

Figure 53: Quantile estimations of total activity on the convex hull of data measurements for the three methods for H1 plan (level -0.5 m) on left (a) and H2 plan (level -1.5 m) on right (b)..... 45

Figure 54: Risk of exceeding the IRAS threshold for the three methods on the total domain area at level -0.5m (H1) and level -1.5m (H2). ..... 46

Figure 55: Risk of exceeding the IRAS threshold for the three methods on the convex hull of data locations at level -0.5m (H1) and level -1.5m (H2)..... 46

## Summary

The INSIDER project (2017-2021) developed and validated a new and improved integrated characterization methodology and strategy during nuclear decommissioning and dismantling operations of nuclear power plants, post-accidental land remediation or nuclear facilities under constrained environments.

One significant part of this project was the implementation on several application cases. This paper is dedicated to the radiological characterization for use case 3a (UC3a) dealing with contaminated soils, in the context of post-incident remediation of a site. For this application case, the constraint environment comes from the difficulty to collect samples beneath a building on the one hand and the fact that samples were collected in the past with no possibility for additional samples. This task has been initiated by gathering prior knowledge for the contaminated site and analysing the available dataset (historical assessment plus available data from on-site measurements and laboratory analyses on destructive samples).

For accessibility reasons to the contaminated soils beneath the building without entering in the building, the measurement campaign uncommonly provided 7 horizontal drill holes of 25 meters on 2 horizontal layers at 0.5 and 1.5 m below lower concrete slab. These drill holes have been measured in laboratory to get about 30 samples on each of them.

Then two evaluation objectives were pursued: global estimates of total activity (source term or radiological inventory) and local categorization of volumes according to a radiological threshold for waste acceptance. Several statistical and geostatistical approaches are compared to quantify the impact of model parameters such as dealing with measurement uncertainty and detection limits, sampling reduction, integration of gamma-scanning as an auxiliary measurement in a multivariate approach, integration of a nugget effect on the variogram... As full part of the INSIDER project, a specific focus is put on uncertainty quantification.

## 1 Annex 3: UC3a Summary

### 1.1 Overall strategy

#### 1.1.1 Request for initial characterization

For some confidentiality reasons the strict minimum of the site context information has been made available within the INSIDER project. However, this situation is sometimes representative of real circumstances for old facilities or legacy sites for instance, for which historical knowledge results are very limited. What can be mentioned is this nuclear facility was devoted to radiochemistry on trans-uranium elements. It was under operation until 1992 on a CEA site in France. The contaminated soil area is located beneath a building, just below a former tank room.

It has been reported that different incidents occurred during nuclear facility operation decades ago. Contamination of soils beneath the tank room with few TBq of various alpha et beta emitters is expected due to:

- Leaks of radioactive very high active effluent in the tank room.
- Several potential contamination pathways to reach the soils such as ingress, cracks or expansion joints of the concrete slab, etc.

In parallel to current decommissioning of the above former nuclear facilities, it is then necessary to characterize these contaminated soils beneath the building.

#### 1.1.2 Define objectives

##### 1.1.2.1 Global estimation of statistical quantities

For the preparation and management of a soil remediation project, some global quantities need to be estimated in a sound way. For instance, average activity concentration value for the whole area (as well as its related uncertainty) is an interesting parameter and needs to be statistically estimated. The different statistical tests and inequalities can be derived if the dataset is compatible with the underlying hypotheses. Spatial and/or statistical biases need to be carefully addressed. Consequently, the **total activity (still along with its confidence level)** can be estimated as an accumulation (knowing the total volume and the matrix density).

Other global statistical quantities are linked to specific values. At that stage, global estimations of volumes exceeding radiological thresholds significantly help for the classification according to the different waste categories.

##### 1.1.2.2 3D distribution map of activity concentration and waste segregation

In addition to the global estimates presented previously, some local estimates are very relevant for the adequate management of remediation projects. The analysis of depth profiles combined with the horizontal distribution leads to 2D/3D representations depending on the dataset spatial organization. Appropriate geostatistical methods need to be carefully selected given the spatial continuity of the phenomenon and the database configuration (linearity, stationarity, multivariate, trend...).

In addition to global estimates, local estimates are expected in comparison to specific radiological values. The local probability of exceeding a radiological threshold then leads to the volumes to be excavated in the different waste categories. At this stage, radiological thresholds for the different waste categories are not yet fully defined, for site release values particularly (output of operator

impact assessment study). For the segregation between Very-Low Level waste and Low-Level waste, as a French site, ANDRA (National Radioactive Waste Management Agency) specifications are quite clear and require a **weighted sum calculation according to scaling factor and nuclide class (IRAS)**.

This classification decision can also take the remediation support into account (e.g. averaging out over 1 m<sup>3</sup> or 1 ton or other values). All classification decisions then require working on estimation uncertainties.

### 1.1.3 Gather pre-existing records/data

In order to develop the radiological assessment of soils below this tank room, different sampling campaigns have been conducted. They consist in 7 horizontal drill holes, the last one was collected a couple of years after the first six ones. As presented on the vertical and horizontal section views on Figure 1 and Figure 2, these drillholes are distributed in two horizontal layers at 0,5m (H1) and 1,5m (H2) below bottom of the tank room slab. Horizontal drilling is not a very common approach for soil sampling but was required due to the site constraints (impossibility to introduce the drilling machine in the building).

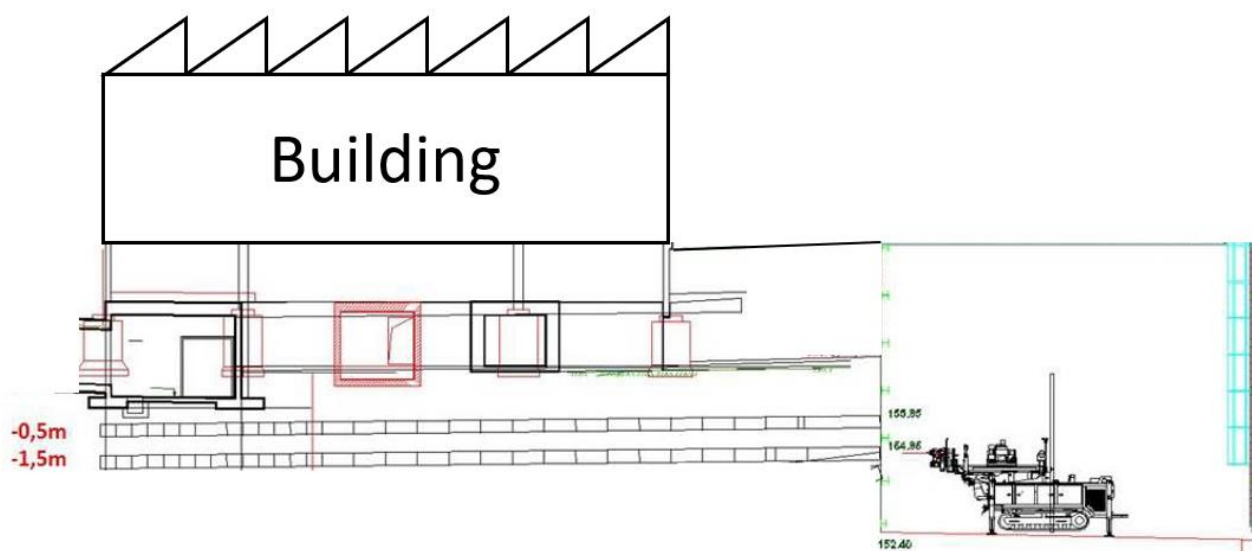
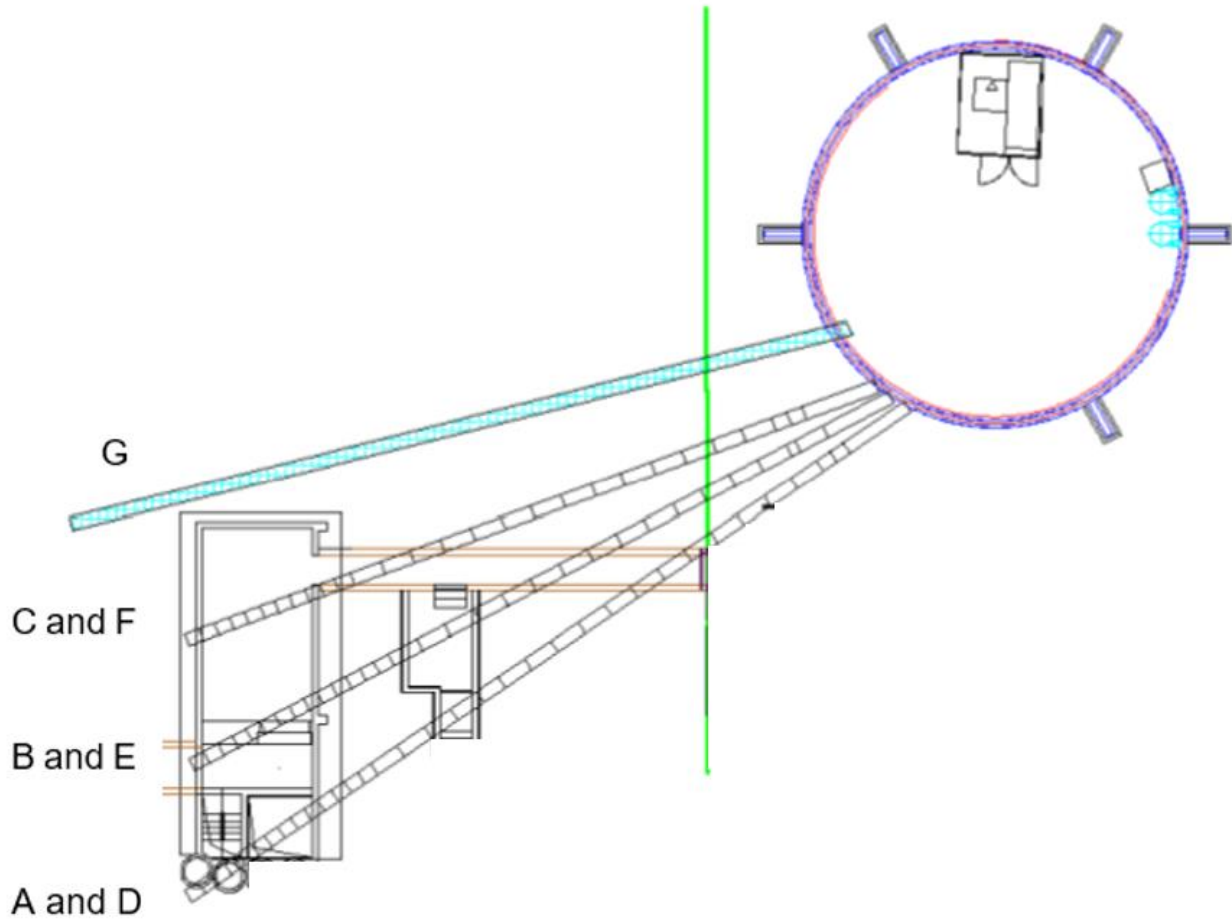


Figure 1: Vertical cross section of the two horizontal drilling layers.



**Figure 2: Top view of the angular distribution of drill holes.**

Samples have been collected using a sonic drilling method that uses high frequency vibration transmitted to the ground via the drill stem and corer. Soil becomes loose or fluid over a very limited area (1 to 5 mm). The main advantage is the rotating corer penetrates soil easily and quickly.



**Figure 3: Sonic drilling machine similar to the one used on UC3.**

As for sampling protocol (cf. Figure 4), it consists in

- Lowering (or pushing) the corer at the sampling depth (distance)
- Retrieving up the corer containing the soil
- Introducing the tube to the depth previously drilled
- Recovering scraps with worm screw
- Repeating these steps until the end of the drilling

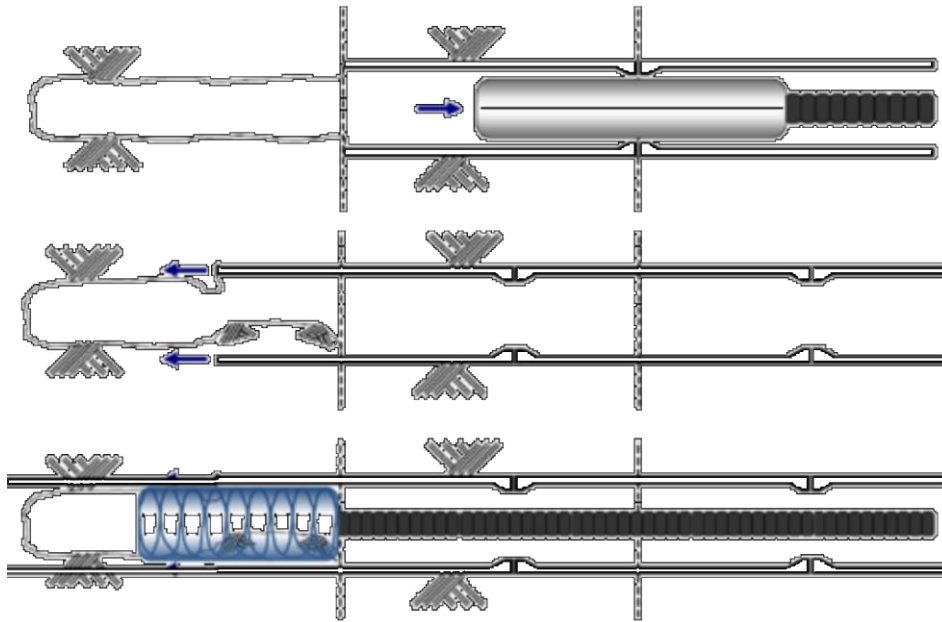


**Figure 4: Different steps for drilling samples.**

Collected soil proved to be quite homogeneous but with the presence of small to intermediate size gravel in a sandy matrix (Figure 5). Samples have been then constituted taking 500 to 800 g mass (geometry standardized at 500 mL) assuming two core lengths: 0,5 or 1 m. First observations of radioactivity distribution depend on soil compositions and radionuclides chemical properties. In addition, activity is concentrated in small soil particles.



**Figure 5: Raw drilling core (top) and result of size segregation (bottom).**

### 1.1.4 Is data sufficient for analysis?

Looking to the spatial organisation, samples were collected along 7 cores, distributed in two layers. The sampling resolution is 1 m and is refined to 50 cm in the interest area (Figure 6). Therefore, the first 10-15 meters from the origin point can be considered as an accessibility distance. The last borehole (named G) is different as it presents a 50 cm sampling resolution from the beginning.

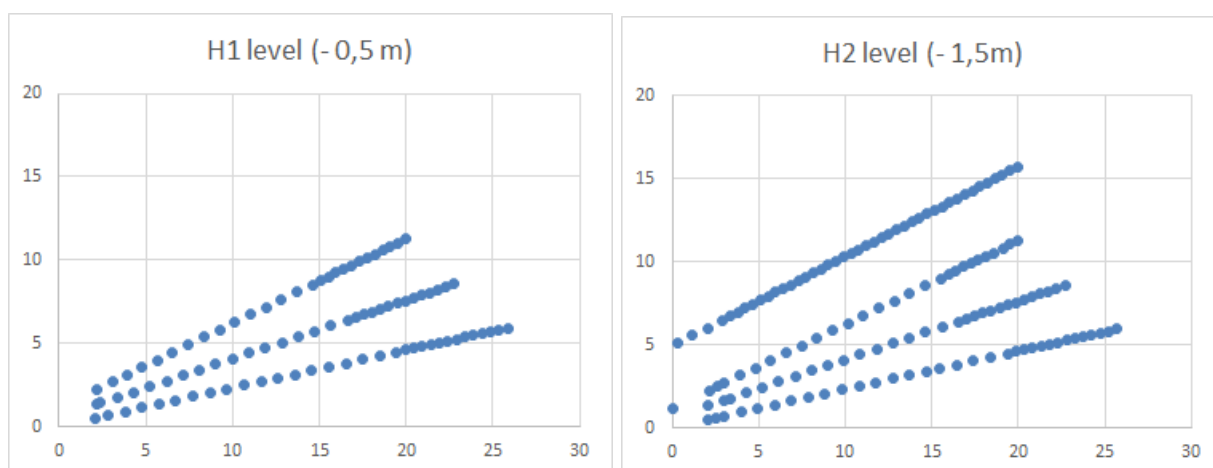


**Figure 6: Base maps of the two sampled layers, H1 on left with boreholes A, B and C, H2 on the right with boreholes D, E, F and G.**

The total number of analysed samples then reaches 220, which can be considered as a large dataset at first glance.

Preliminary direct measurements have been performed along the cores. They consist in gamma and X scanning (gross counting) on a regular 5 cm mesh (Figure 7). These indirect measurements probably serve as a semi-quantitative characterisation of the gamma content of soil samples. This “on-site” secondary data will be advantageously used within the INSIDER project to be able to combine in-situ and destructive values in order to improve the estimations (and reduce the uncertainties).

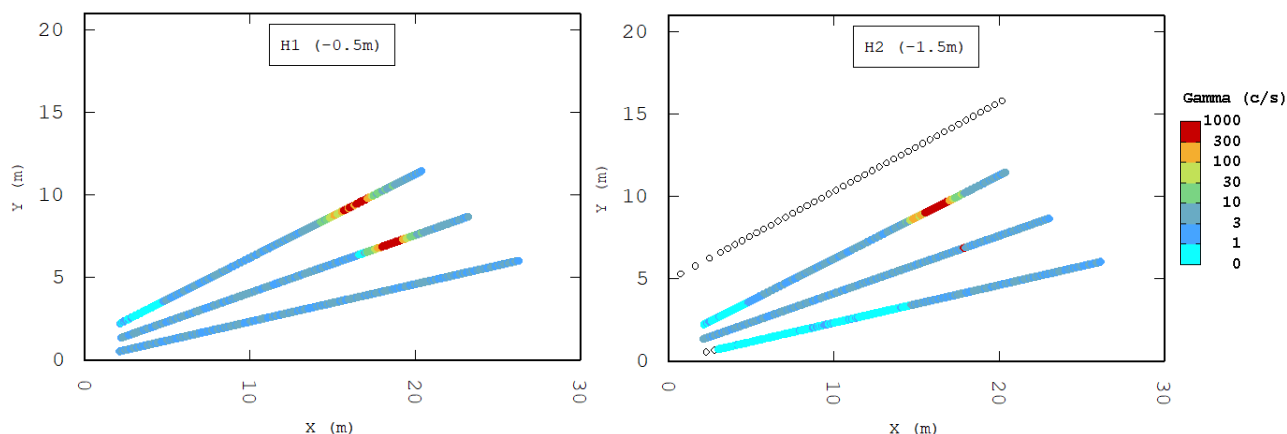


**Figure 7: Base maps of gamma scanning for level H1 at -0.5m (left) and H2 at -1.5m (right). No gamma scanning was performed on borehole G.**

Laboratory analyses were performed for alpha, beta and gamma nuclides. Still for confidentiality reasons only the three main nuclides are kept and anonymised. They will be arbitrary named A, B and C through the rest of the document.

It seems that alpha spectrometry (dissolution, extraction, electrodeposition) and beta counting (liquid scintillation with a detection limit of 30 Bq/kg) have been initially decided on the basis of the higher dose rate location on the core. At the end, most of all samples have been measured for alpha emitters and only the first layer of boreholes (3 out of 7) for nuclide B.

### **1.1.5 Can more samples be collected?**

As there is no possibility for new samples and new in situ measurements, the existing dataset is considered as the final one within the INSIDER project for this use case 3. However, non-destructive measurements and new samples can be performed on the existing cores.

There is no sampling design definition as for the other use cases, but the statistical analysis promises to bring interesting and relevant conclusions for the whole INSIDER project due to the number of available samples. Global and local estimates will be calculated as requested in §1.1.2.

In addition, sensitivity to dataset extension will be studied as 2 zones can be identified: the inner area with the highest activity levels (corresponding to the 50 cm sampling resolution along the cores) and the accessibility area (with a 1 m mesh). Statistical outputs will differ because of this spatial delineation.

As it seems to be a relevant 3D contamination, areas with high estimation uncertainties as well as extrapolation areas will finally be identified. They would have been used for recommendations of new samples in the case of a site with possible additional investigation.

Despite the dataset limitations for the definition of the sampling plan as described before, the large number of samples enables a sound sensitivity analysis. Sub-dataset will be extracted from the full dataset in order to quantify the impact on the estimates and their related uncertainties. Different possibilities can be imagined:

- Reduction of sample number per drill hole.
- Integrating correlation between nuclides by reducing some laboratory analyses.

This approach will definitely provide interesting outputs for the INSIDER project.

## 1.2 Data analysis & sampling design

Still for confidentiality reasons, activity concentrations for radionuclides A, B, C are multiplied by different coefficients beforehand. So the presented values are not the real ones but all statistical and geostatistical methodologies remains valid. Only the IRAS (French acronym for radiological limit between very low level waste and low level waste) analysis (§1.2.3.4 and §1.2.4.2) is biased by these coefficients. Other results and conclusions are consistent.

### 1.2.1 Pre-processing and exploratory data analysis

Percentages of data above quantification limits are studied on the three nuclides for further statistical and geostatistical calculations. In the input file, the quantification values are reported when the measurement result was not significant. They are latter named limits of detection (LOD).

As reported in Table 1, there are still many data, which are not detectable value. Their proportion is from 39% for nuclide B in the plan H1 (-0.5m) to 81% for nuclide C in the plan H2 (-1.5m).

**Table 1: Proportion of valid data and LOD for each radionuclide and each plan H1 (-0.5m) and H2 (-1.5m).**

Nuclide	Layer H1 (-0,5m)				Layer H2 (-1,5m)				Total valid
	Valid		LOD		Valid		LOD		
A	31	35%	58	65%	51	38%	82	62%	82
B	54	61%	35	39%	42	32%	91	68%	96
C	26	29%	63	71%	25	19%	108	81%	51

Figure 8 shows the histograms of the three main radionuclides, displaying data below (blue) and above (green) quantification limit. As the three statistical distributions are very skewed, a logarithm scale is used.

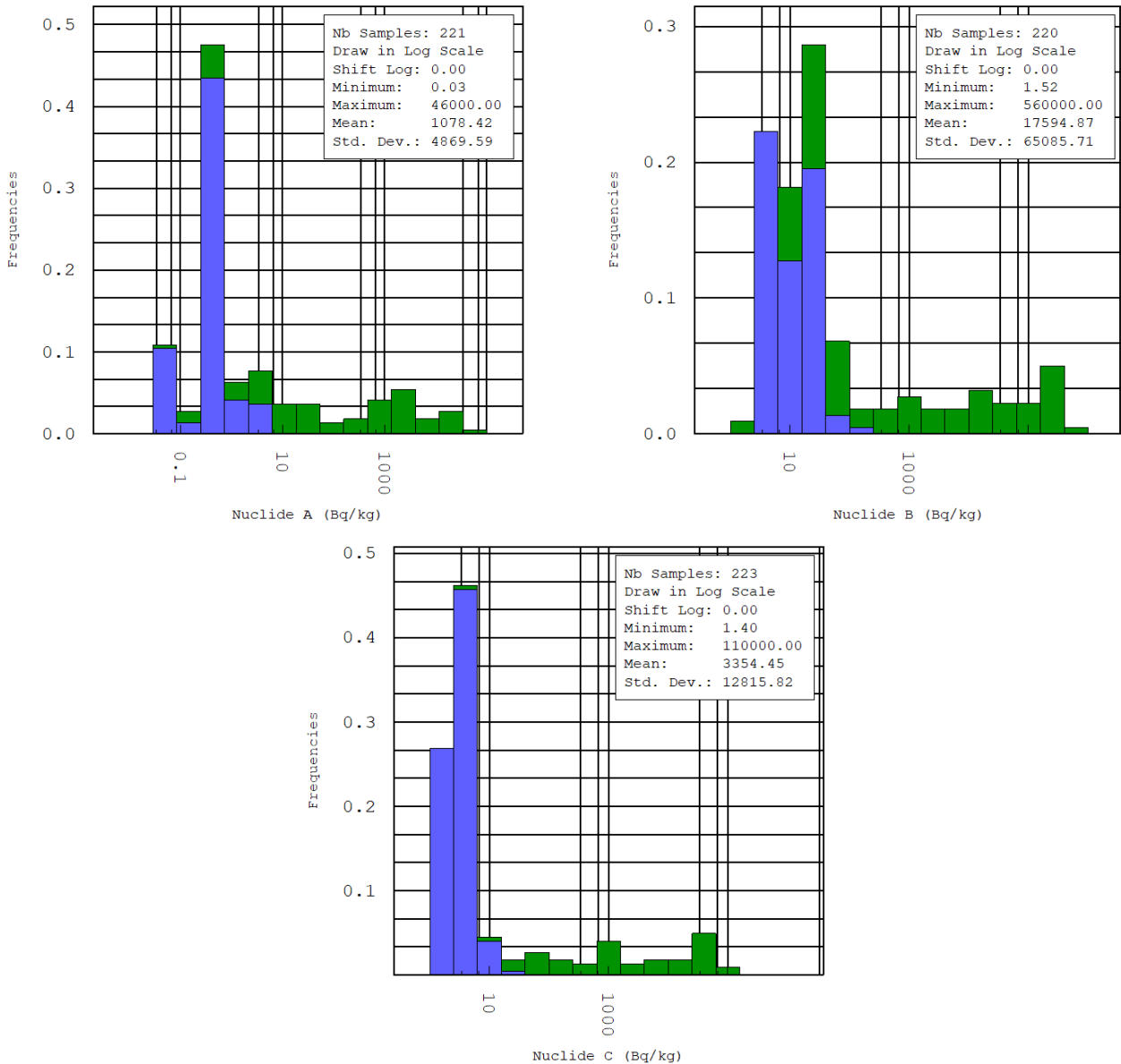


**Figure 8: Histograms of the three nuclides (Bq/kg). In blue: data below quantification limit.**

Figure 9 shows the histograms for the dispersion of relative uncertainties for the three nuclides.

- For nuclide A, 222 spatial data are available that include 82 valid data and 138 censored data (62%) corresponding to limit of detection which are variable from 0.3 to 2.5 Bq/kg. Valid data are associated with uncertainty measurements from 1.4% to 82% and a mean of 33%.
- For nuclide B, 222 spatial data are available that include 96 valid data and 127 censored data (57%) corresponding to limit of detection which are variable from 1 to 105 Bq/kg. Valid data are associated with uncertainty measurements from 1.7% to 240% and a mean of 42%.
- For nuclide C, 222 spatial data are available that include 51 valid data and 171 censored data (77%) corresponding to limit of detection which are variable from 1.4 to 22.5 Bq/kg. Valid data are associated with uncertainty measurements from 8% to 141% and a mean of 19%.

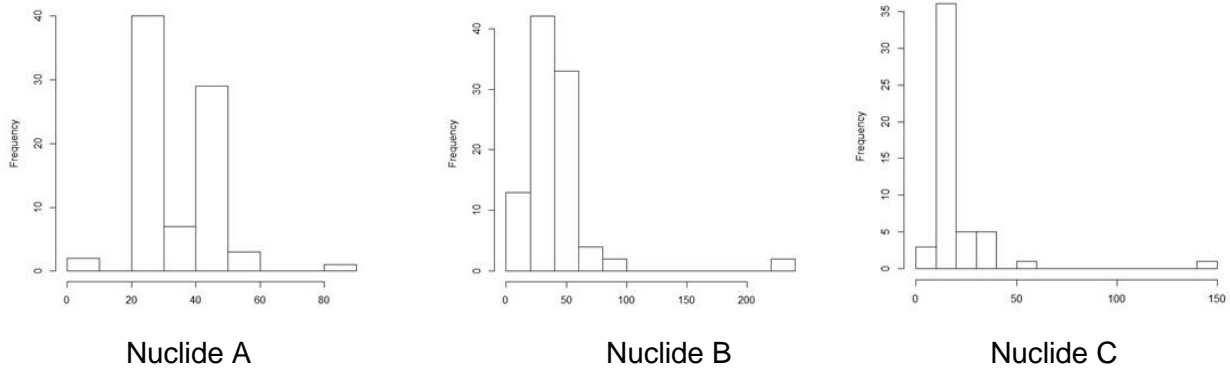


**Figure 9: Histograms for the uncertainties of the three main radionuclides.**

Data quality control is mainly performed by looking at scatter plots between radionuclides and their uncertainties on one hand and between radionuclides on the other hand. Graphics of Figure 10 show clouds between uncertainties and measurement, revealing:

- a probable erroneous value for nuclide C (circled in red) with a x10 factor missing for the measurement (also seen on the correlation between nuclides A and C),
- two different situations for nuclides A and B that could be explained by different conditions during sampling or laboratory analysis and lead to a cloud showing two lines.

As they are not in crucial ranges of activity concentration for the next steps, and due to the fact there is no possibility to check the real values, these points have been kept as they were. However, the correction of these inconsistencies would be preferable prior to further calculation.

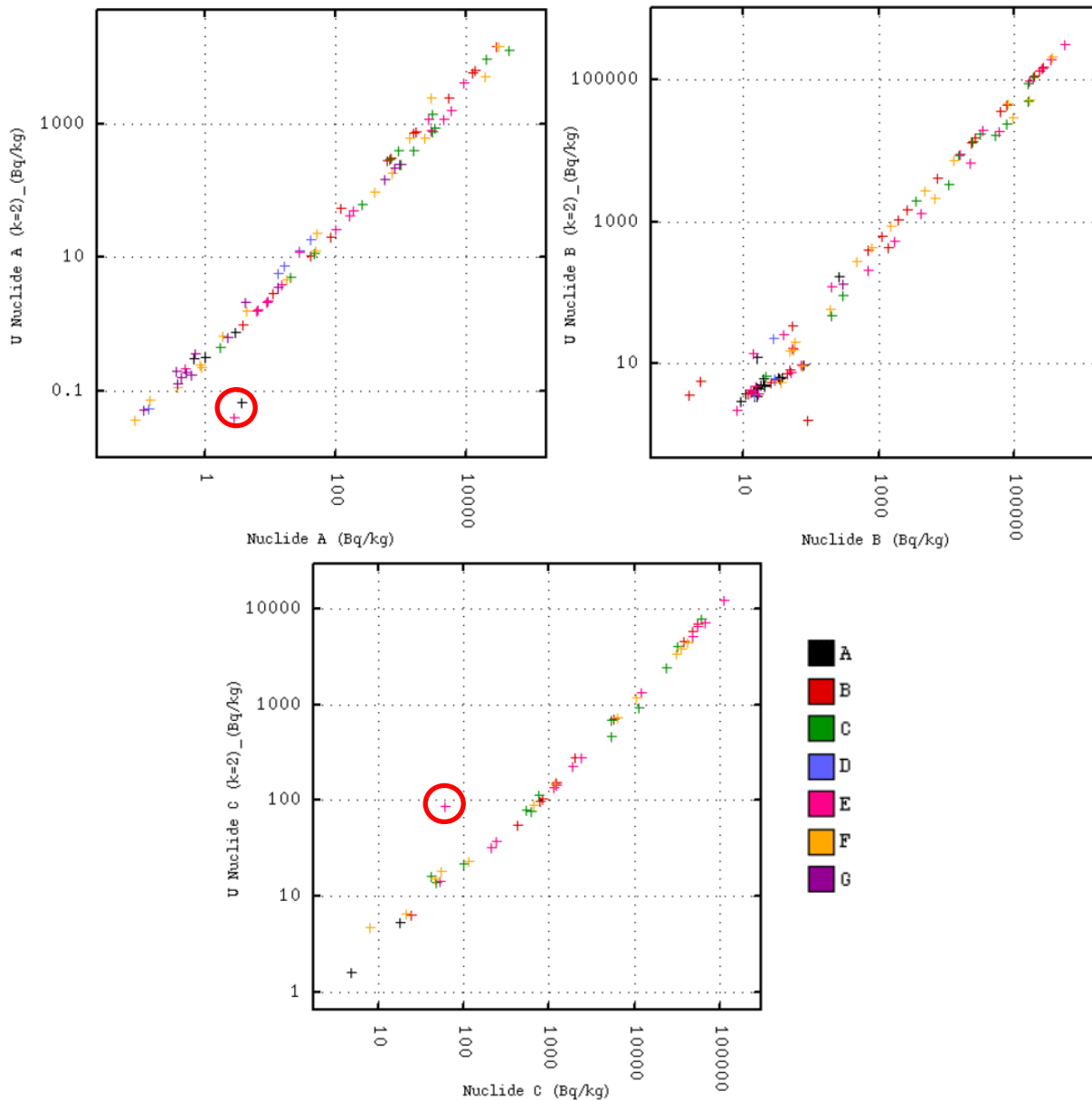


**Figure 10 : Correlation (log scale) between measurement and related uncertainty for the three nuclides (Bq/kg). Identification of outliers. Colorscale related to borehole ID.**

Correlations between all radionuclides are represented on Figure 11. Nuclide A, B and C show high correlations that will be taken into account during the variographic analysis from a spatial point of view (cross variograms) and then for building a multivariate model.

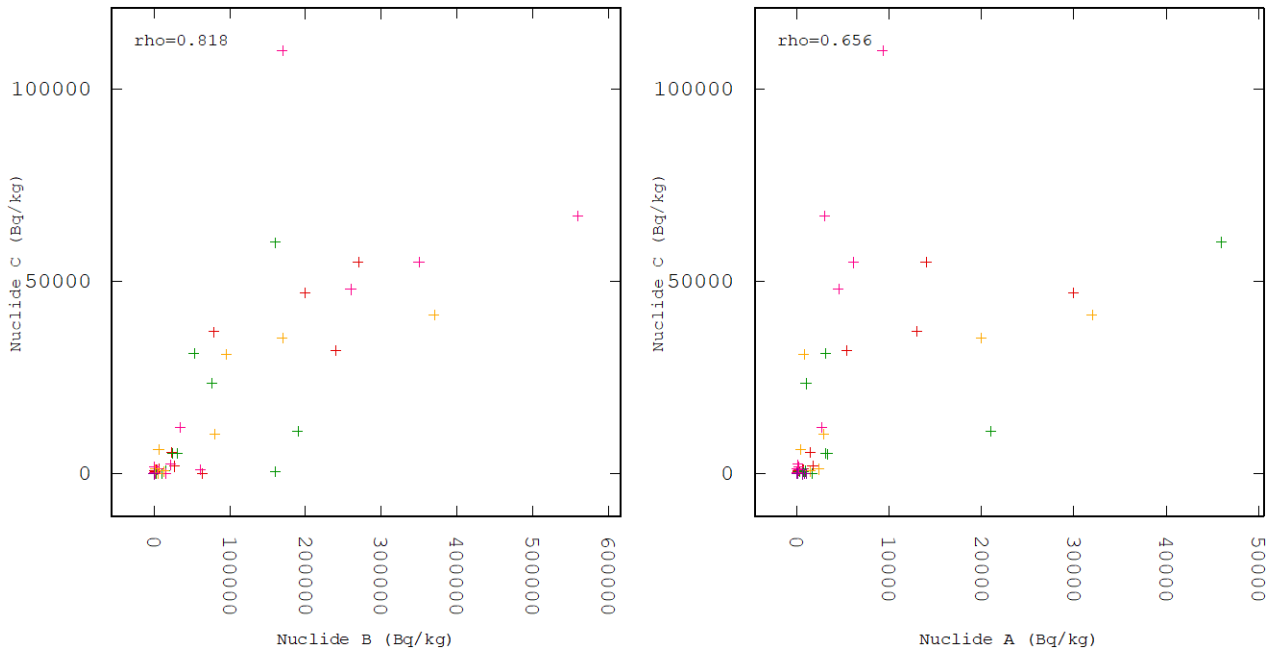


**Figure 11: Linear correlation coefficients between radionuclides A, B and C.**

## 1.2.2 Data analysis and modelling

### 1.2.2.1 Variographic analysis and variogram model

Prior to the variography analysis, it has been decided to work on transformed variables:

- The raw data presents a very skewed statistical distribution (histogram) that requires a data transformation for a suitable and efficient geostatistical processing;
- Logarithmic values are first computed for better robustness of the fitting of extreme values (both flat part around quantification limits and high slope for highest values); and
- The second step consists in transforming the log distribution into a Gaussian one (Figure 12) using Hermite polynomial expansion (normal score transformation of Gaussian anamorphosis).

As a consequence, non-linear geostatistics can be developed (geostatistics simulations in particular). In the radiological characterisation framework, this normal score transformation is systematically used due to the distribution dissymmetry. It generally strongly improves the spatial structure interpretation and gives access to more advanced results such as waste classification (probability of exceeding a threshold).

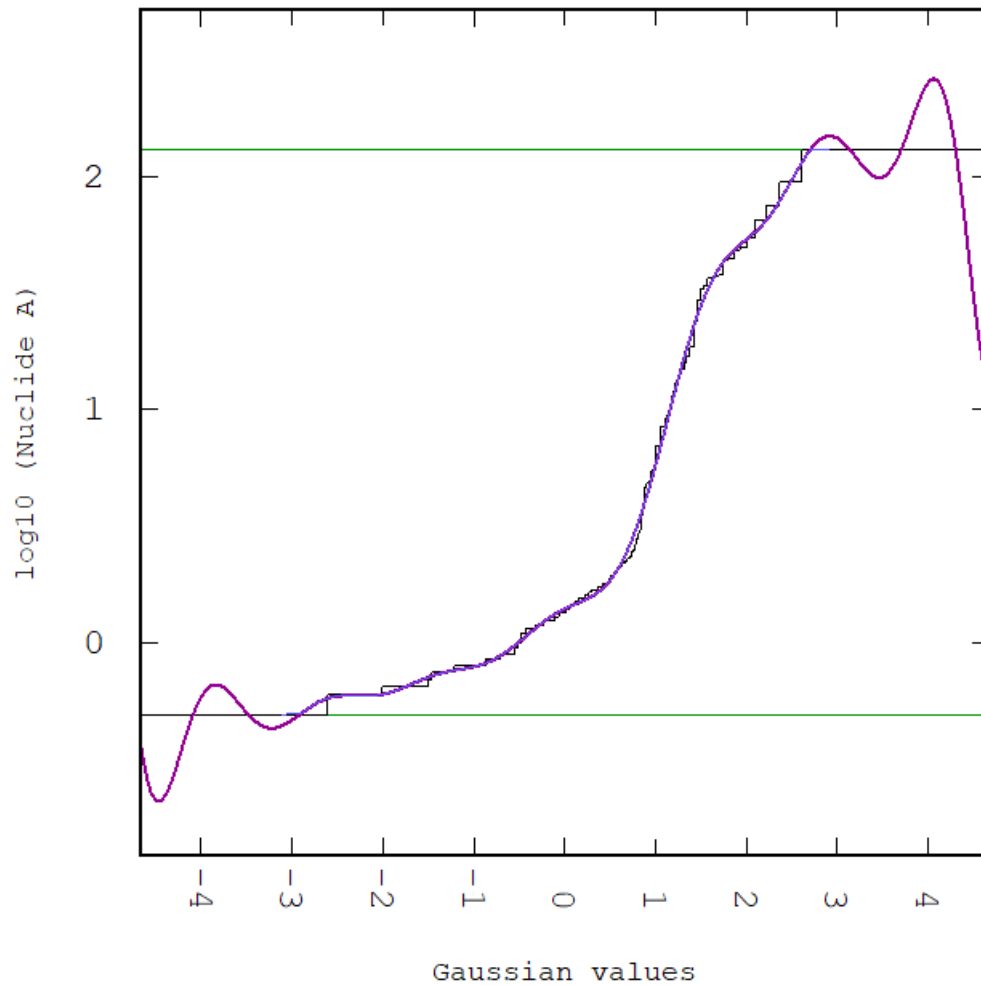


**Figure 12 : Gaussian anamorphosis of log10 transformed data for nuclide A.**  
**This bijection between real distribution (Y axis) and corresponding Gaussian transformation (X axis) enables more advanced geostatistical analysis and results.**

Experimental variograms are computed for all three variables at the same time and for several directions (Figure 13): N60°, N150° and the vertical direction. Directions are chosen accordingly to the main directions of the drill holes which is N60°. In accordance with the sampling, the lag is taken equal to 1m and variograms are calculated up to 15 m. Clear border effects can be seen on the variograms due to the organization of the samples along the drill holes: number of pairs available for the N60° direction is much higher than the one of N150° direction. Regarding the vertical variogram, only two layers are sampled making it difficult to build a relevant vertical variogram. For these two reasons it is decided to fit an omnidirectional model (Figure 14), only based on the N60° experimental variogram, assuming that the contamination has an isotropic behaviour.

The variograms are fitted with two spherical structures with ranges of 5.5m and 15m; sills are reported in Figure 15. This model constitutes the reference case and simulations are going to be done with two 2D layers. In addition, these two ranges are consistent with typical distances for soil contamination extent.

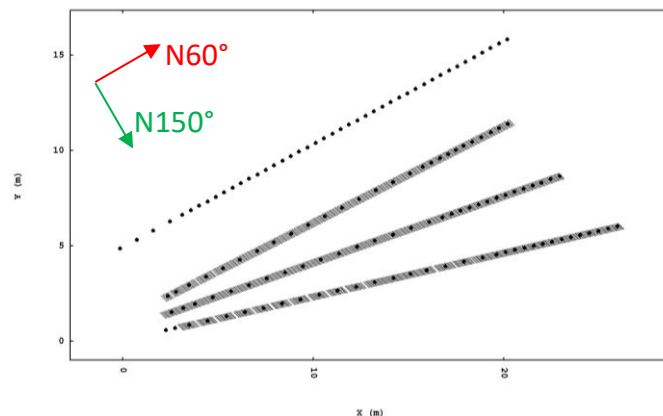


**Figure 13 : Multivariate (nuclides A, B and C) experimental variograms with two horizontal directions and vertical. Top right base map explains orientation in the horizontal plane. The 3 simple variograms are on the diagonal and the 3 cross-variograms in the bottom left part.**

**Figure 14 : Fitted multivariate omnidirectional variogram.  
Dashed line on cross-variograms represents the maximum correlation envelope.**

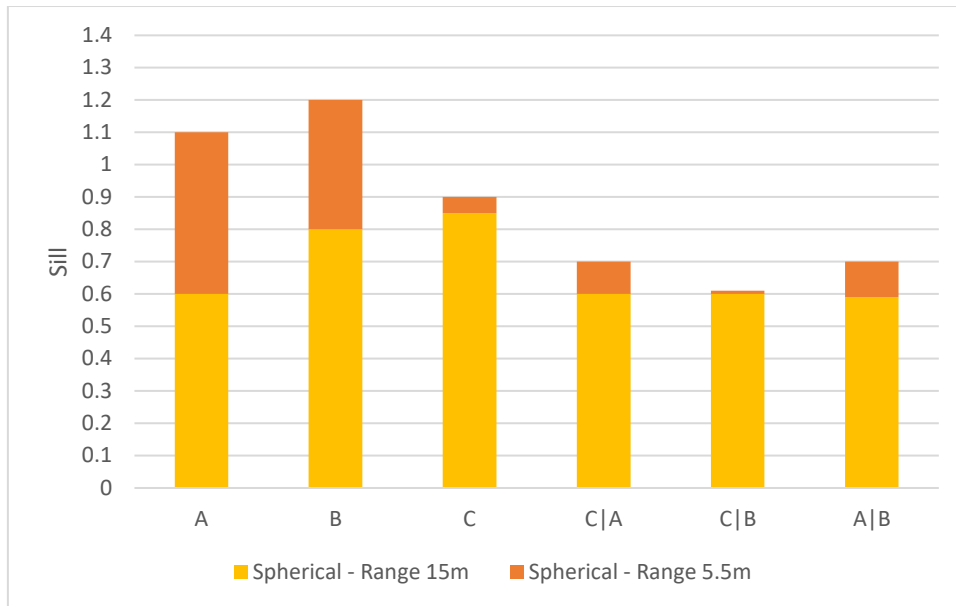


**Figure 15: Model structures and sills for multivariate reference case.**

In order to study the impact of the variogram model on the different estimates (mean, standard deviation maps, accumulations, probabilities to exceed thresholds...), a second variogram model is built (Figure 16). Same structures and ranges are kept but it now includes a nugget effect representing 15% of the total variability (i.e. statistical variance, 1 in the present case due to the normal score transformation).

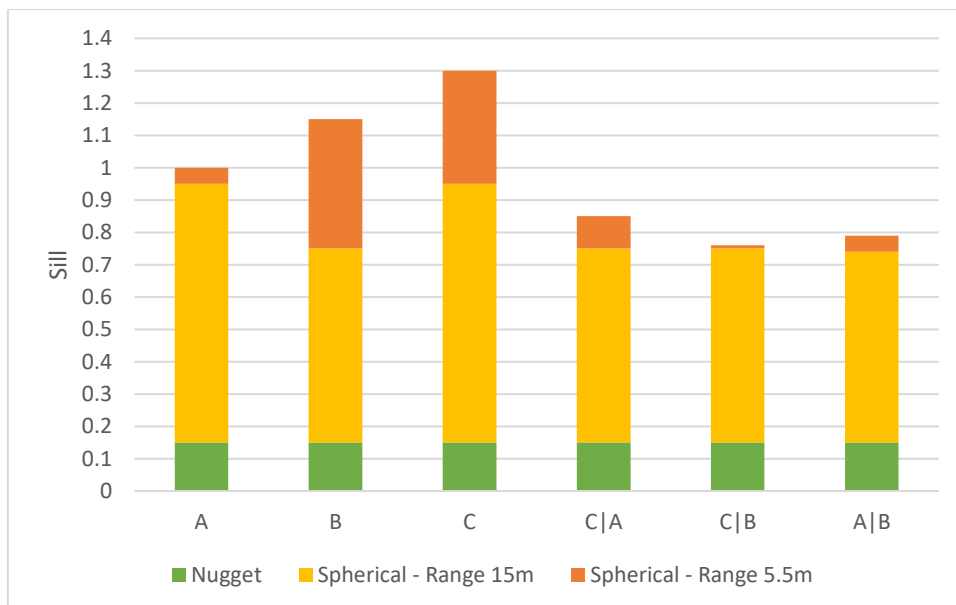


**Figure 16 : Model structures and sills for the case integrating a 15% nugget effect.**

Finally, a third model is built so as to integrate gamma scanning in the estimations. Sills are displayed in Figure 17 (multivariate approach combining in-situ measurements and in-lab results on samples).

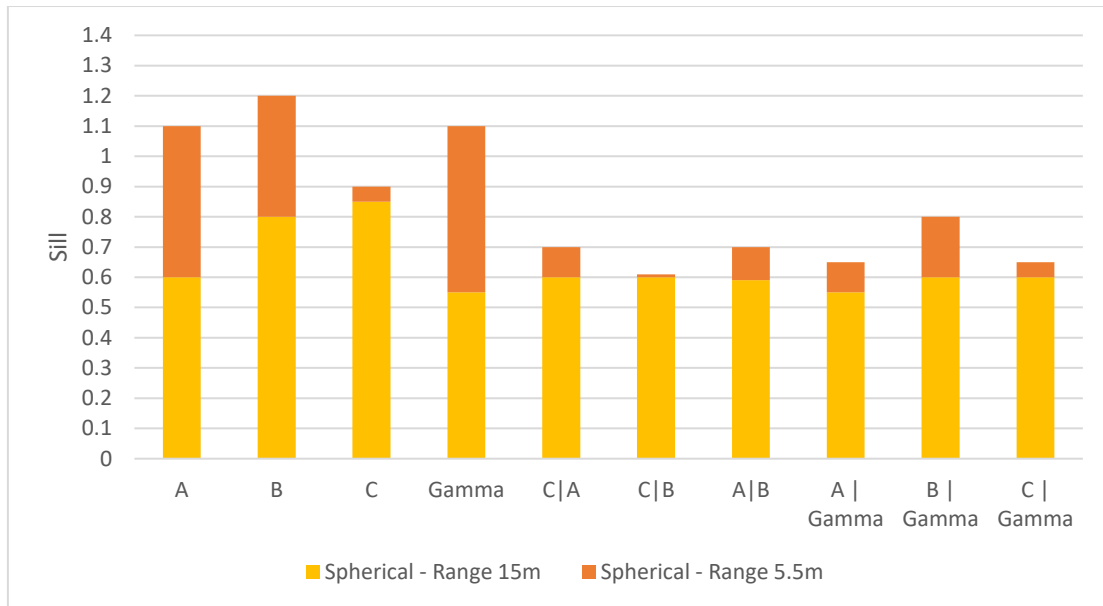


**Figure 17 : Model structures and sills for the multivariate case with Gamma scanning.**

**1.2.2.2 Geostatistics model variants and subsampling variants**

Three variogram model variants have been described in the previous paragraph. Added to these, one more model taking into account all data but with 3D simulations instead of two 2D layers is added as well as several models considering partial datasets of sample results:

- Subsampling every 1m (so removing one point out of two in the inner part of the contaminated area, and thus correcting partially the spatial sampling bias),
- Subsampling every 2m, making possible 2 variants (Figure 18),
- Subsampling every 4m, making possible 4 variants (Figure 19).

For each subsampling, computations are made with or without Gamma scanning. The different base maps clearly point out the fact that medium or high values can be missed with these subsampling and that for the same number of samples results may be different.

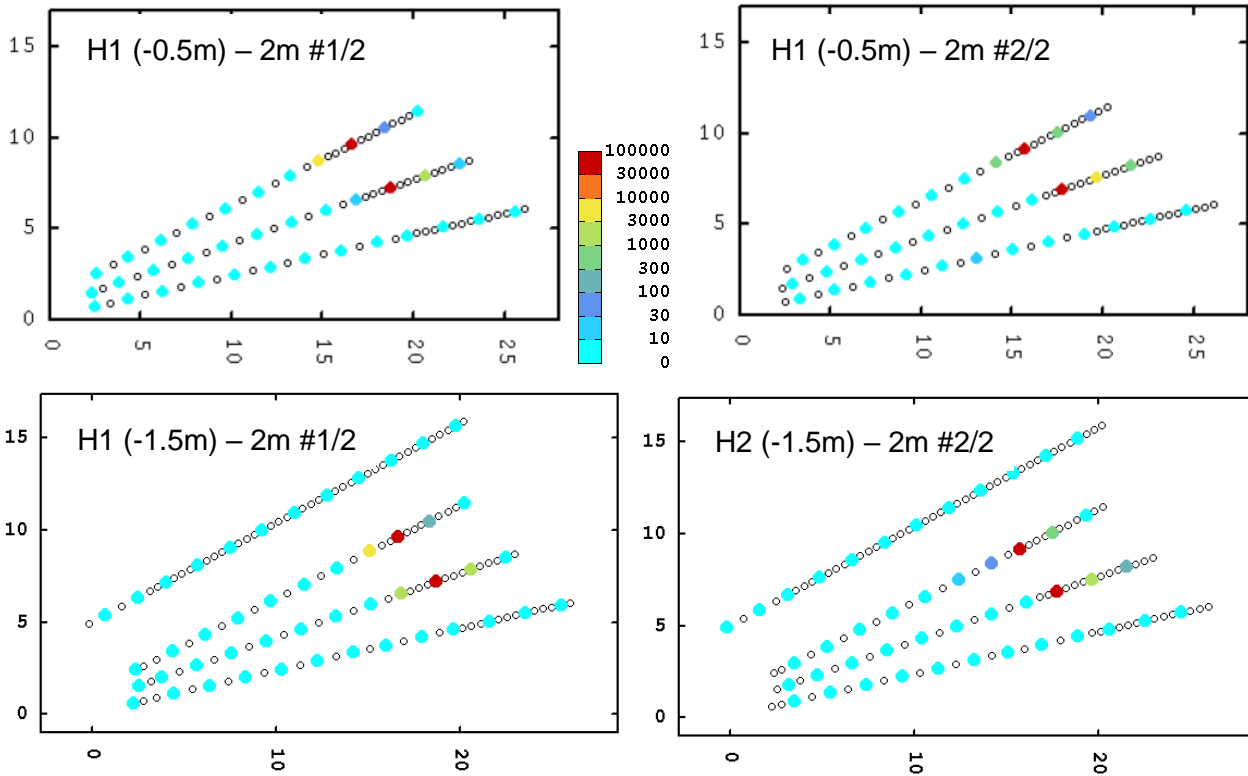


**Figure 18 : 2m subsampling variants #1/2 (left) and #2/2 (right). Black circles are removed data points. Colorscale for nuclide C (Bq/kg).**

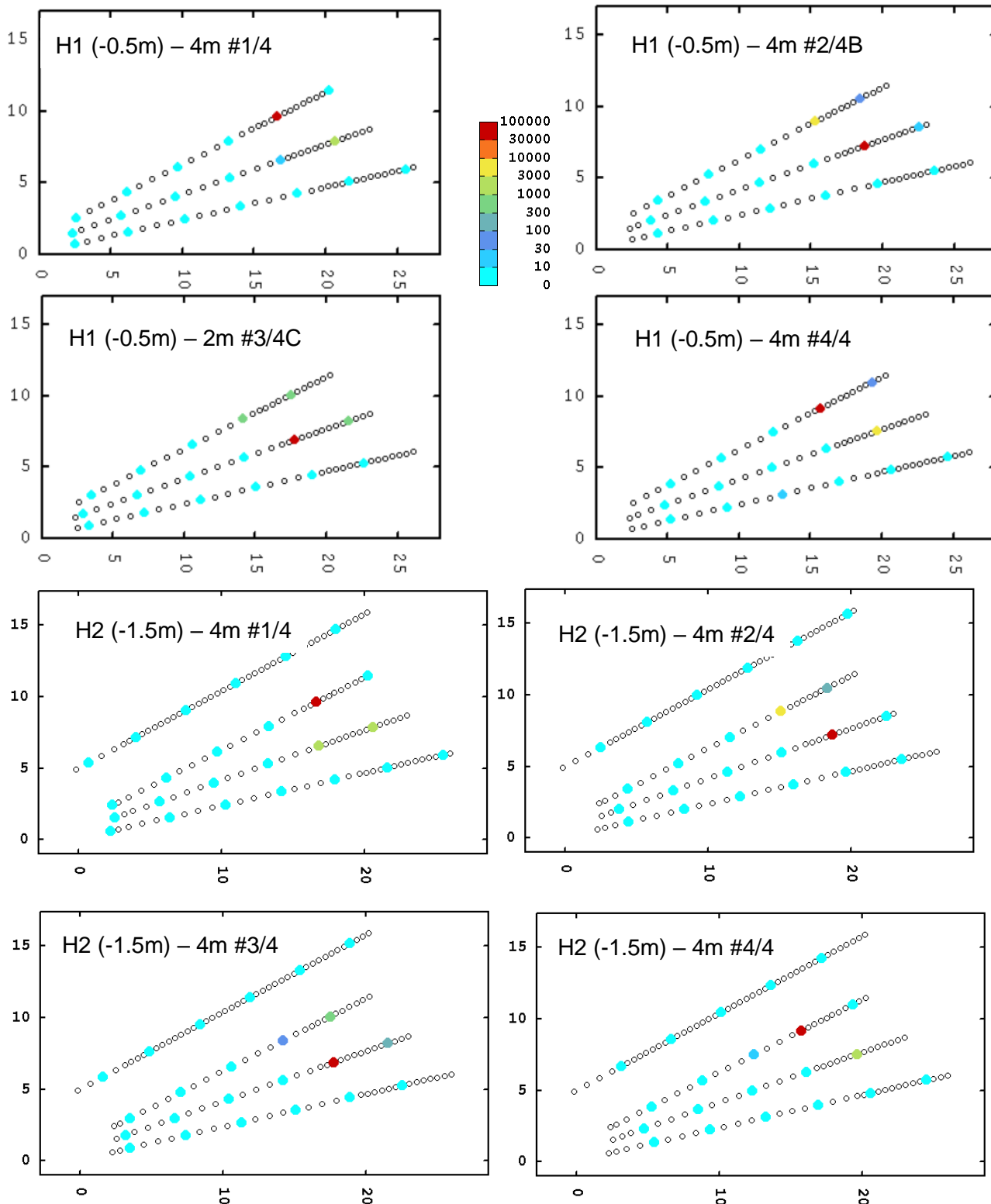


**Figure 19: 4m subsampling variants #1/4, #2/4, #3/4 and #4/4. H1 (-0.5m) on the upper part, H2 (-1.5m) on the lower part. Black circles are removed data points. Colorscale for nuclide C (Bq/kg).**

In the end, 9 major variants have been generated and described in Table 2.

**Table 2: Synthesis of geostatistics model variants and subsampling variants.**

Variant	Samples	Gamma scanning	Variogram	2D/3D	Colour on graphics	Comment
Reference case	All	No	1 <sup>st</sup> model	2D	<b>Bold black</b>	
Nugget effect	All	No	Including nugget	2D	Black	
+Gamma scanning	All	Yes	Including Gamma	2D	Red	
3D	All	No	1 <sup>st</sup> model	3D	Green	
Subsampling 1m	Subsampled every 1m	No	1 <sup>st</sup> model	2D	Yellow	
Subsampling 2m	Subsampled every 2m	No	1 <sup>st</sup> model	2D	Blue	2 possibilities
Subsampling 2m + Gamma scanning	Subsampled every 2m	Yes	Including Gamma	2D	Purple	2 possibilities
Subsampling 4m	Subsampled every 4m	No	1 <sup>st</sup> model	2D	Grey	4 possibilities
Subsampling 4m + Gamma scanning	Subsampled every 4m	Yes	Including Gamma	2D	Brown	4 possibilities

Corresponding results are presented in §1.2.3.

### **1.2.2.3 Geostatistical and statistical approaches, sensitivity to limits of detection and measurement uncertainties treatment**

In addition, outcomes from innovative statistical and geostatistical methodologies developed by CEA (FRANCE Patent No. 1906548, 2019) (FRANCE Patent No. Demand in progress, 2020) makes it possible to exploit different kinds of data as valid measurement data, uncertainty measurements and limits of detection. The aim is to use incomplete information in censored data as uncertainties and limits of detection to reach realistic characterization estimations. Usually measurement uncertainties are not considered or as systematic uncertainties in geostatistical approaches. They are treated by a nugget effect or by a heteroscedastic term in classical geostatistical models. For data lower than limits of detection (LOD), the standard practice is to take the value equal to decision threshold which is LOD/2 as valid data. Furthermore, this methodology proposes objective confidence criteria to evaluate the estimation quality. This approach is all the more important when measurement uncertainties are high, and/or proportion of data that are under the limit of detection is important, as it is presently the case with this study. Throughout this document, results from three approaches will be compared to assess the relevance of treating specifically limits of detection and measurement uncertainties considering the targeted objectives:

- Classical geostatistical approach with a fitted spherical variogram without nugget effect; LOD are treated as valid data and uncertainty measurements are not taken into account: called *Geo*;
- Geostatistical approach with a specific treatment of LOD and uncertainty measurements with at the end of the method a fitted spherical variogram without nugget effect: called *Geo+LOD+U*;
- Probabilistic modelling approach with a specific treatment of LOD and uncertainty measurements with a fitted lognormal probabilistic distribution with parameters that are function of position: called *PM+LOD+U*.

Corresponding results are presented in §1.2.4.

A preliminary analysis has been performed to assess the validity of normality hypothesis on natural logarithmic transformation of data. The validity of this hypothesis is important for the next steps of the studied methodologies, in particular for conditional simulations in geostatistical approaches. The normality analysis concerns only valid data considering that limit of detection data have been modified and contain an incomplete information on the real value.

Table 3 shows that the normal hypothesis is largely respected by all data sets except for nuclide B on plan H1 (-0.5 m) but the p-value is very close to 5%, so the normal hypothesis can reasonably be assumed for all that will follow.

**Table 3: Normality statistical test analysis on valid data.**

Log(Activity)	Normality tests on valid data			
	Anderson-Darling Test		Cramer-Von Mises Test	
	H1	H2	H1	H2
Nuclide A	p-value=0.57	p-value=0.51	p-value=0.51	p-value=0.53
	not-rejected	not-rejected	not-rejected	not-rejected
Nuclide B	p-value=0.04	p-value=0.17	p-value=0.05	p-value=0.2
	rejected	not-rejected	not-rejected	not-rejected
Nuclide C	p-value=0.74	p-value=0.68	p-value=0.76	p-value=0.7
	not-rejected	not-rejected	not-rejected	not-rejected

### 1.2.3 Post-processing with geostatistics model variants and subsampling variants

#### 1.2.3.1 Geostatistical simulations

Several sets of 500 simulations corresponding to the different models and subsampling cases have been launched. Several maps and indicators can then be derived from the simulations. Figure 20 and Figure 21 show the mean and standard deviation of all the simulations for the reference case. All maps and results are given considering an estimation grid with cells of 1m<sup>3</sup> (1x1x1m) that represent the remediation decision unit (for soil excavation and waste packages). For both levels, highest contamination is located just under the tank room whereas very low levels occur at the beginning (left) of the drill holes. However, contamination estimation and uncertainty are very different between levels in the upper part of the site. Medium values are estimated for level H1 (-0.5m) whereas it corresponds to low values for level H2 (-1.5m). Uncertainty is also much higher in the first case. This is explained by the fourth drill hole made only for level H2 (-1.5m) which shows very low values and allows a much better delineation of the contamination. The contamination delineation can be improved on level H1 (-0.5m) by considering the 3D-model; results will be compared in terms of accumulation and probability to exceed a threshold.

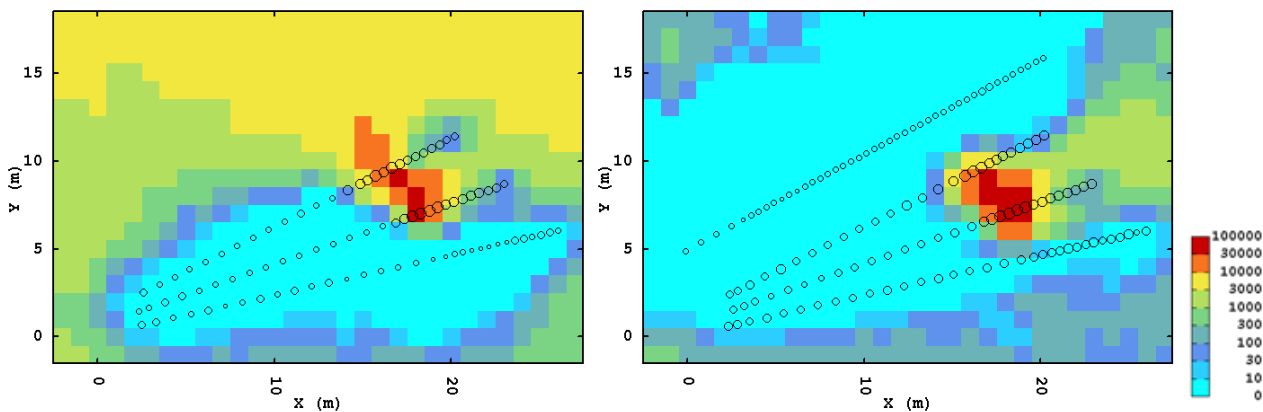


Figure 20: Mean of 500 simulations for Nuclide C (Bq/kg). Left: H1 (-0.5m); right: H2 (-1.5m).

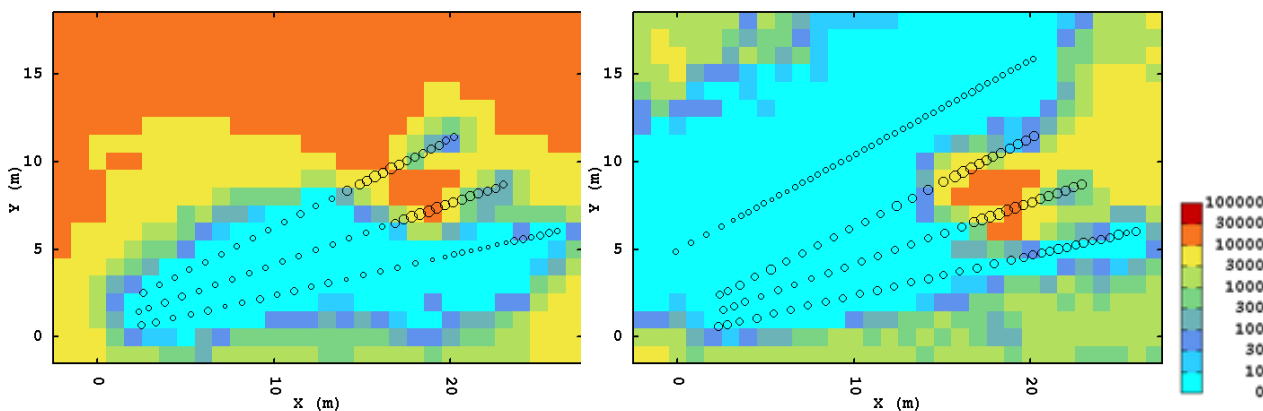


Figure 21: Standard deviation of 500 simulations for Nuclide C (Bq/kg). Left: H1 (-0.5m); right: H2 (-1.5m).

### 1.2.3.2 Total activity (source term or radiological inventory)

As a global post-processing of geostatistical simulations (statistical distribution of the average concentration of each individual stochastic realisation), Table 4 gathers total accumulation estimations for nuclides A, B and C as well as uncertainty quantifications.

**Table 4: Total activity for the three main nuclides (GBq) for the reference case and for levels H1 (-0.5m) and H2 (-1.5m).**

Total activity (GBq)		Estimation (Q50)	Confidence interval [Q5 - Q95]	Dispersion coefficient [Q95-Q5]/Q50
H1 (-0.5m)	Nuclide A	<b>0,59</b>	0,21 - 2,58	4,02
	Nuclide B	<b>6,02</b>	2,34 - 30,23	4,63
	Nuclide C	<b>1,67</b>	0,48 - 7,67	4,31
H2 (-1.5m)	Nuclide A	<b>0,18</b>	0,09 - 0,55	2,56
	Nuclide B	<b>4,75</b>	2,8 - 10,86	1,70
	Nuclide C	<b>0,81</b>	0,51 - 1,32	1,00

For comparison purpose, only total activity linked to nuclide C has been computed for all variants. Resulting graphs are presented in Figure 22 to Figure 24. Figure 22 represents the complete

statistical distribution of total activity as a global estimate for each variant and each level whereas the two other figures facilitate the comparison.

For level -0.5m, the clear impact comes from the 3D variant. Without considering the neighbour points from the second level and especially the additional drill hole in the upper part, total accumulation ranges from approximately 0.14 GBq to 12.41 GBq (5% and 95% quantiles). It appears that in the upper part (Figure 20), contamination is overestimated due to extrapolation (at large distance, the spatial estimation tends to the statistical mean, which is biased due to the sampling spatial configuration). If there was no other level, area to be mapped should be reduced to avoid this.

Other comparisons are therefore made on level H2 (-1.5m) where there is one more drill hole enabling to considerably decrease the values and uncertainties in the upper part of the site.

For this level (Figure 22 and Figure 24), results of reference case, subsampling at 1m and the 3D variant are close. Adding gamma scanning decreases the total activity (it was also possible to see it for level H1 at -0.5m) as well as adding a nugget effect on the variogram (extreme values are smoothed with nugget effect whereas they have the largest contributors to the accumulation for total activity estimation). Except for the variant with the nugget effect, uncertainty is the same for all these variants; it is larger when considering a nugget effect which was expected as it adds variability for small distances.

Regarding subsampling, 1m subsamples give results very similar to cases taking into account all samples. However, more differences can be seen with 2m and even more for 4m subsampling. Some of these subsampling variants may give consistent results as regard reference scenario but it is very depending on samples that are kept (in particular for extreme values that significantly impact the nuclide inventory). As seen on Figure 18 and Figure 19, results highly depend on the samples that are selected or not. Figure 24 also shows that results can be worse for 4m subsampling in terms of uncertainty and variability. For those subsampling variants, adding gamma scanning usually give results with less uncertainty and smaller total activity.

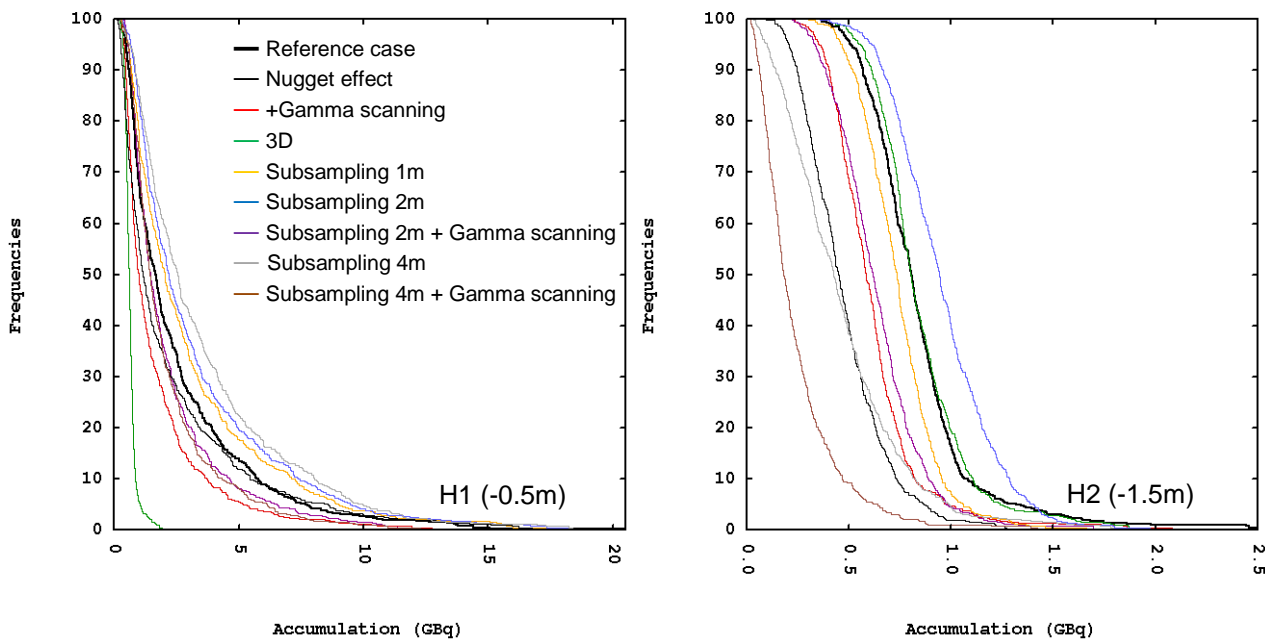


**Figure 22: Total activity for nuclide C (GBq), levels H1 at -0.5m (left) and H2 at -1.5m (right) depending on the variant.**

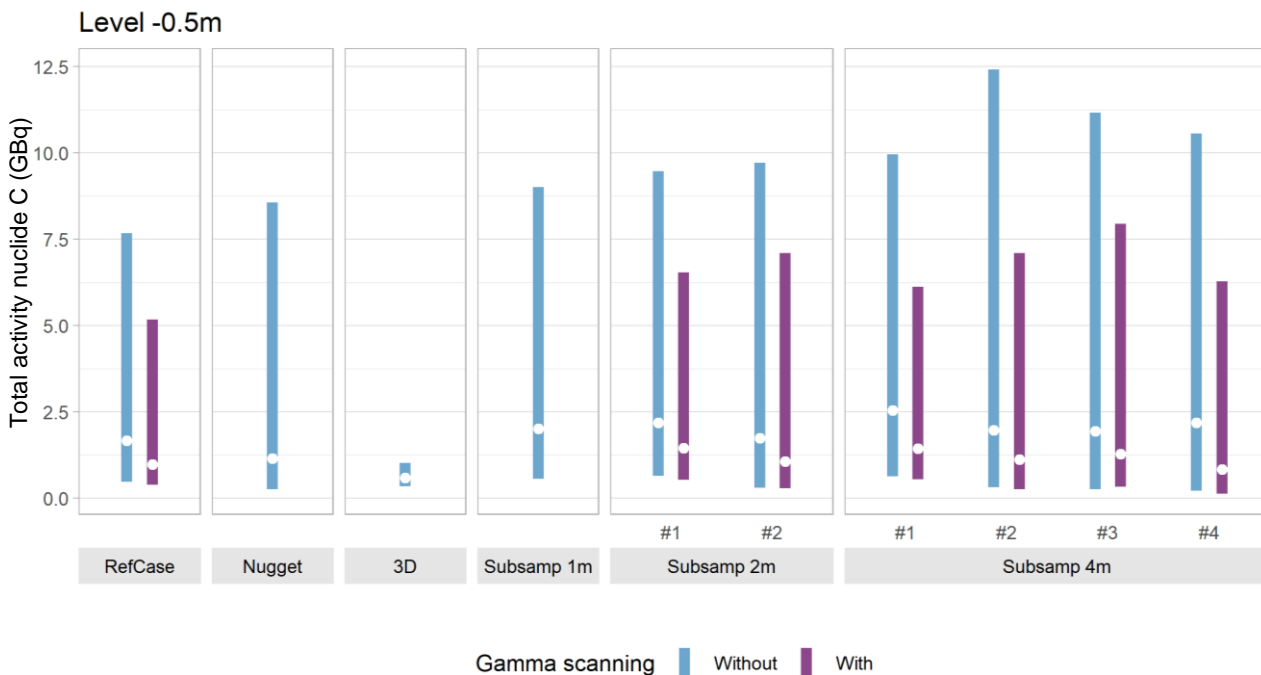


**Figure 23: Median and 90% confidence interval for nuclide C total activity depending on the variant, Level H1 (-0.5m).**

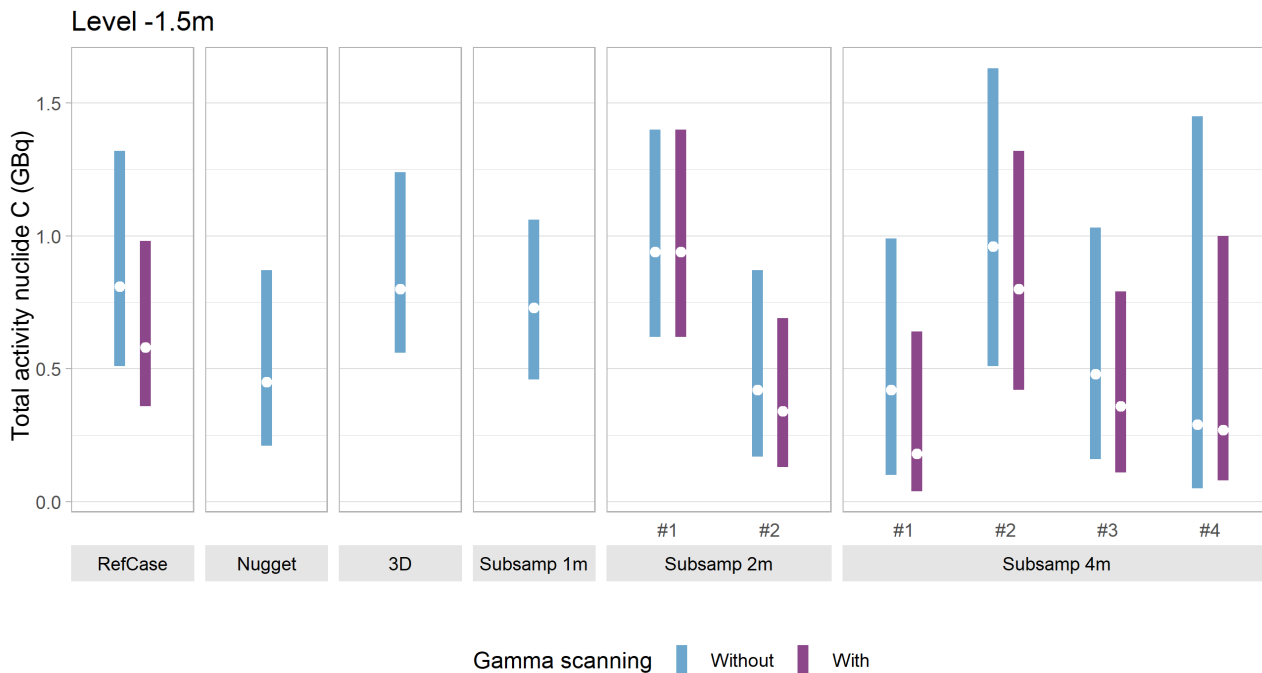


**Figure 24: Median and 90% confidence interval for nuclide C total activity depending on the variant, Level H2 (-1.5m).**

**1.2.3.3 Probability to exceed a threshold close to the Quantification Limit (QL)**

Probability to exceed a threshold is also computed in order to estimate the volumes to be excavated according to radiological criteria. In this chapter, several thresholds have been tested for nuclide C to study how corresponding volumes increase when the threshold decreases. This sensitivity analysis is performed to study the issue of having thresholds that can be very close to quantification limits.

Histograms of Figure 25 display values below and above QL. QL is usually lower than 10 Bq/kg but can sometimes reach more than 20 Bq/kg. To test the effect of the threshold on remediation volumes knowing these QL, several thresholds have been tested ranging from 10 to 1000 Bq/kg.

Figure 26 and Figure 27 represent the different quantiles for remediation volumes depending on the chosen threshold, using the reference case model. For both levels there is a clear and expected exponential increase of remediation volumes when the threshold is very low and close to the QL. Results of level -0.5m are again greatly influenced by the large part of the site that is extrapolated. However, for level -1.5m (H2), it is possible to see that the influence is even more larger for very small thresholds. Increase of remediation volumes for 20 and 40 Bq/kg is even faster than an exponential curve.

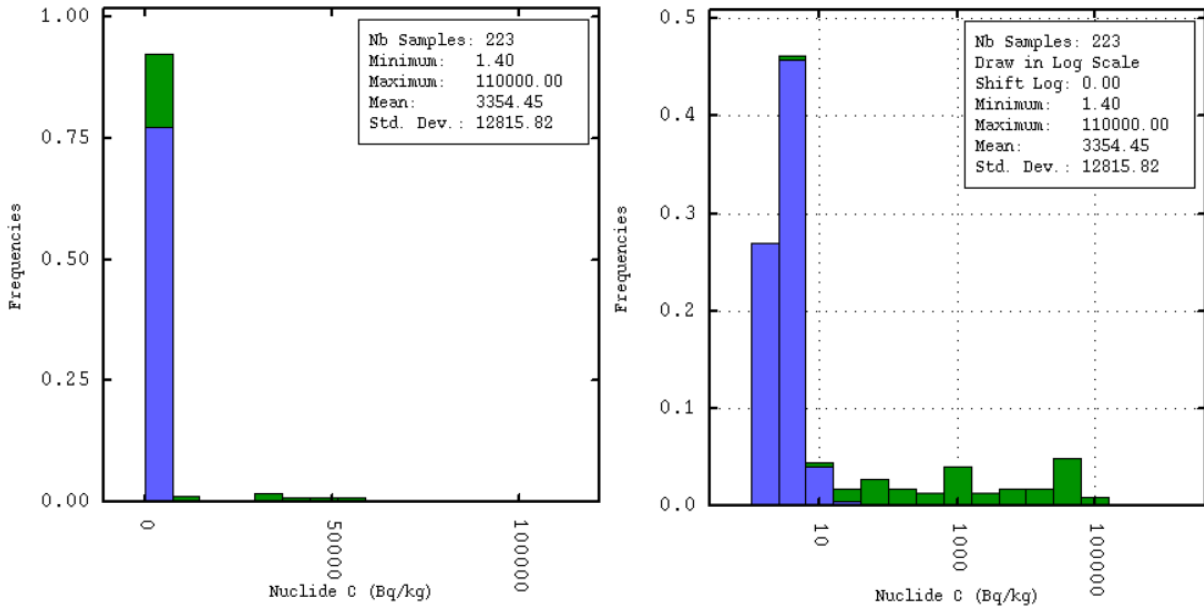


**Figure 25 : Raw and logarithmic histograms for nuclide C showing values inferior to QL in blue.**

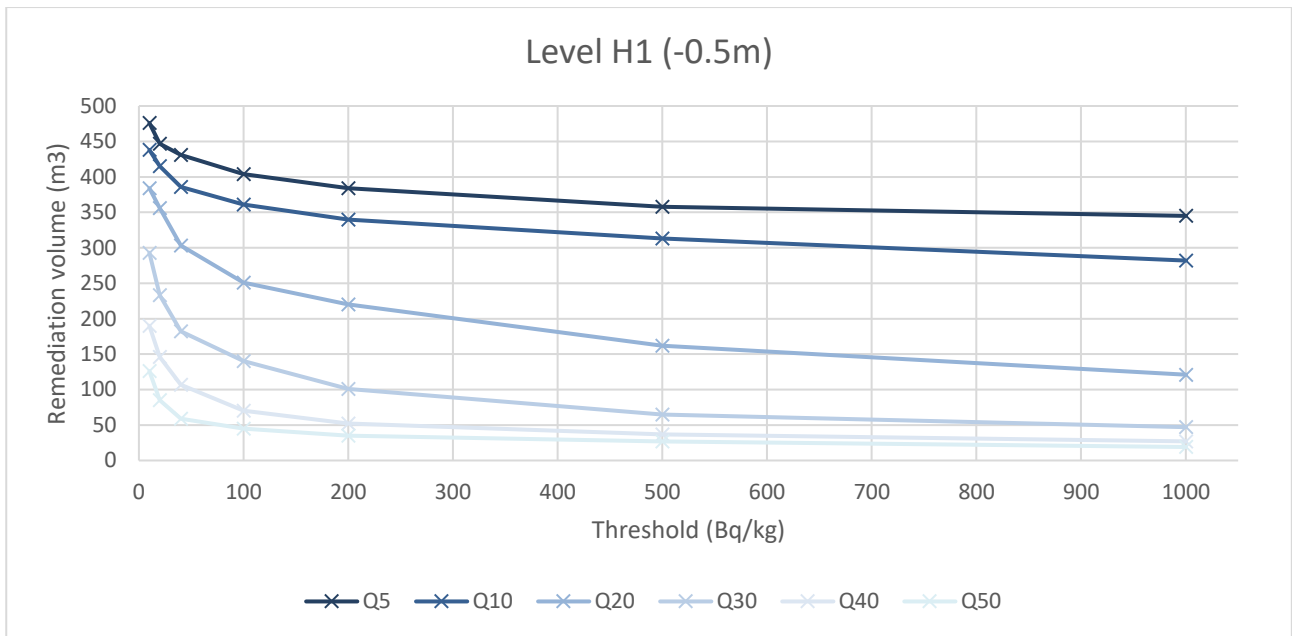


**Figure 26: Evolution of remediation volumes linked to nuclide C contamination depending on the threshold and for different risks (quantiles), Level H1 (-0.5m).**

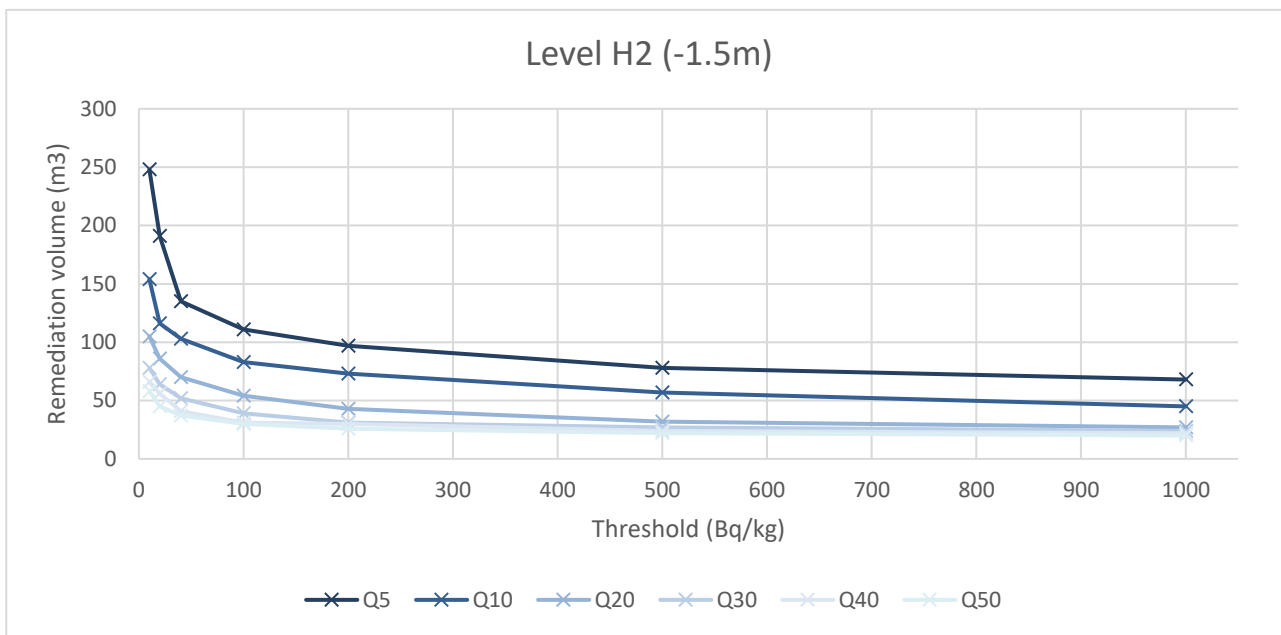


**Figure 27: Evolution of remediation volumes linked to nuclide C contamination depending on the threshold and for different risks (quantiles), Level H2 (-1.5m).**

**1.2.3.4 Probability to exceed IRAS threshold**

For the segregation between Very-Low Level waste and Low-Level waste, remediation volumes are computed using the IRAS threshold (waste acceptance criteria), as follows:

$$\frac{\text{Nuclide A}}{10} + \frac{\text{Nuclide B}}{1000} + \frac{\text{Nuclide C}}{10} \geq 1$$

Like total activity calculations, all 17 variants of the model have been tested and results are gathered in Figure 29 and Figure 30. Figure 28 enables a direct comparison of selected variants for the two layers (only 1 subsampling dataset is kept for a specific distance). For level H1 at -0.5m, 3D variant gives significantly lower remediation volumes thanks to the additional drill hole of the second level. Other effects are clearer for level H2 (-1.5m) and are detailed below.

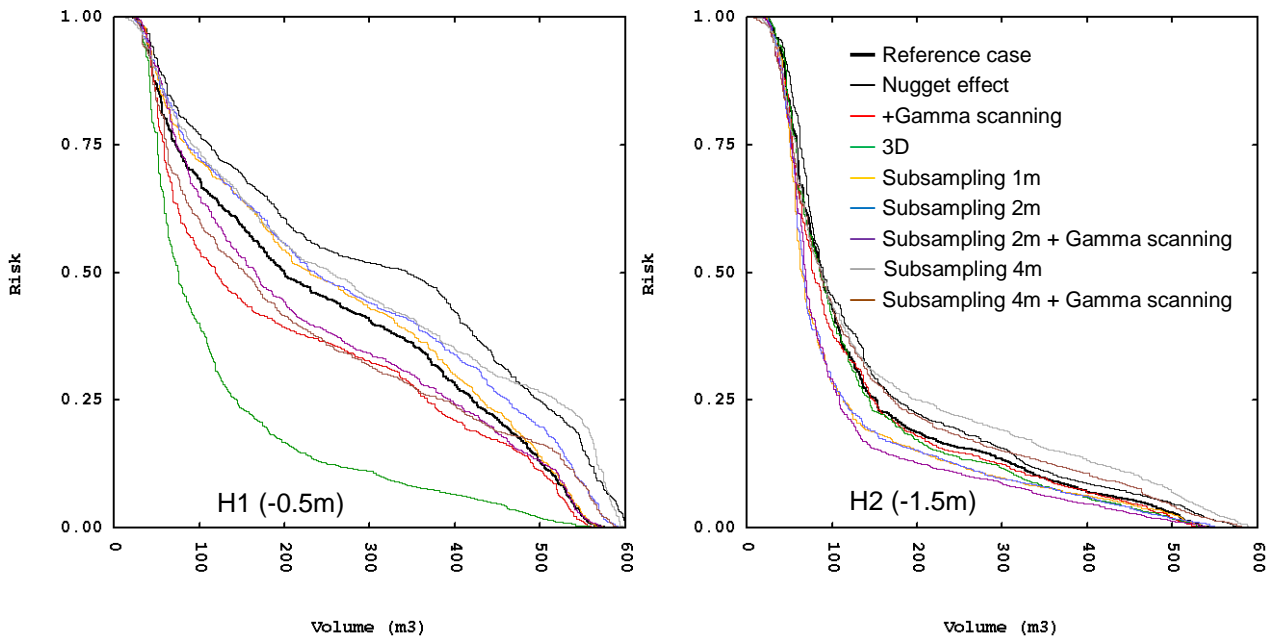


**Figure 28: Remediation volumes for IRAS threshold depending on the variant, levels H1 at -0.5m (left) and H2 at -1.5m (right).**

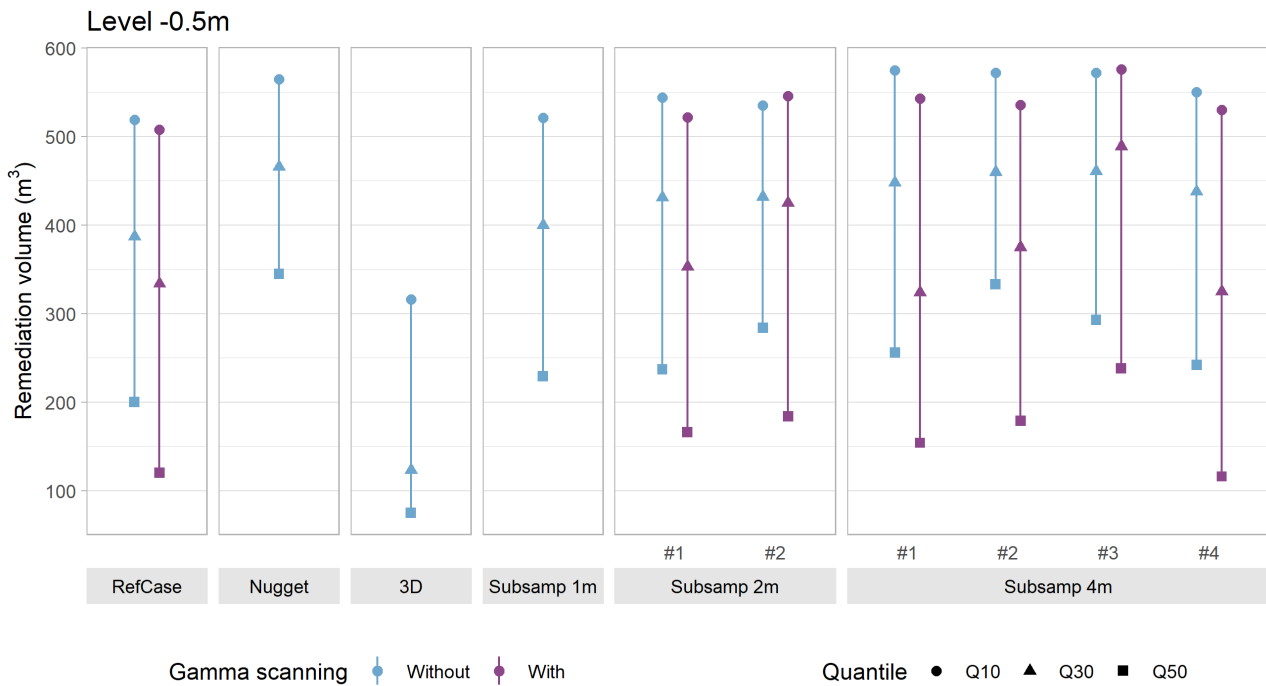


**Figure 29: Remediation volumes for IRAS threshold depending on the variant and for different risks (quantiles Q10 – Q30 – Q50), Level H1 at -0.5m.**

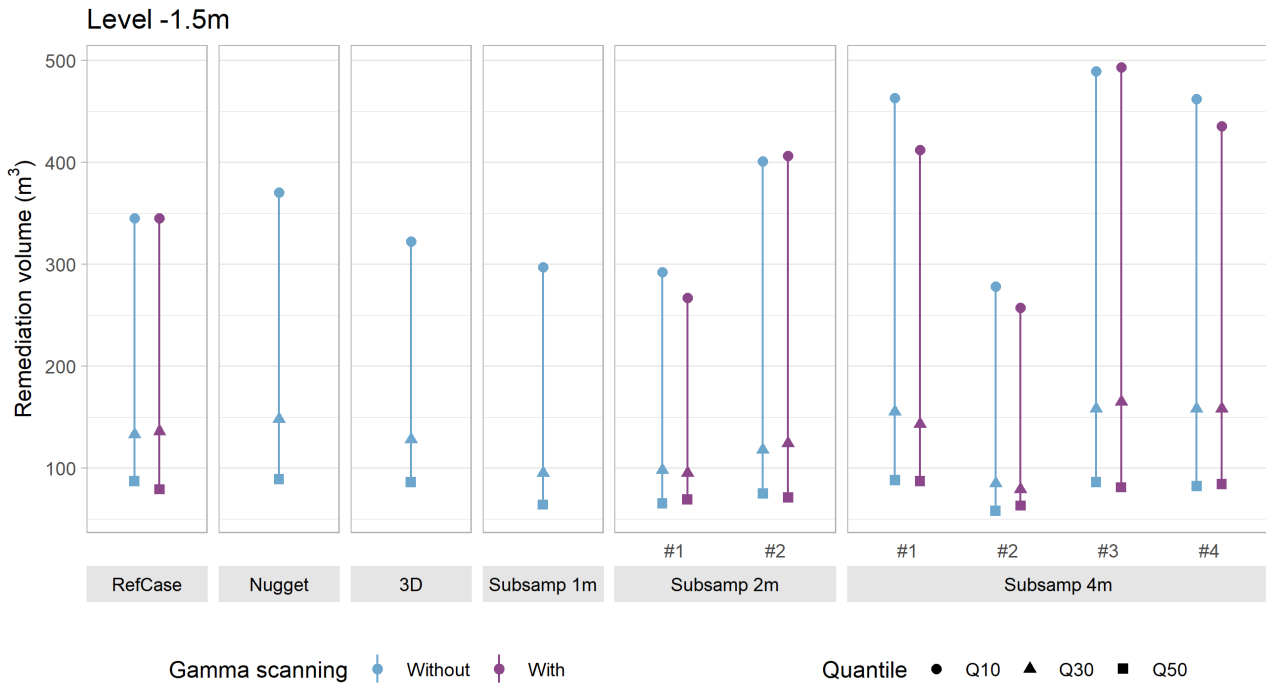


**Figure 30: Remediation volumes for IRAS threshold depending on the variant and for different risks (quantiles Q10 – Q30 – Q50), Level H2 at -1.5m.**

First effect is that the differences between variants are larger for small risks like 5 or 10% than for large risks like 50% (only for H1 (-0,5m) layer). However, results remain globally consistent and robust.

Regarding the 4 first variants, main effect is observed for the model with the nugget effect (Figure 31), which corresponds for this example to larger remediation volumes for a given risk. Subsampling at 1m also gives results close to the reference case. As already seen for total activity estimation (§ 1.2.3.2) the 3D variant gives better estimates at H1 level (-0,5m depth) due to the extra drill hole at -1,5m (H2 level).

However, results become much more erratic (but with limited deviations) with subsampling at 2 or 4m, giving remediation volumes that can be a little bit lower or greater than those of the reference case. Depending on samples kept, the variability in the results can be very large, considering gamma scanning or not. For example, Figure 32 displays the map for two 4m-subsamplings: delineation of areas with 5, 10 or 20% of risk is very different depending on the samples but is not very much impacted by the use of gamma scanning (unfortunately using gamma scanning does not compensate the lack of information here, probably because gamma scanning is also made along the drill holes).

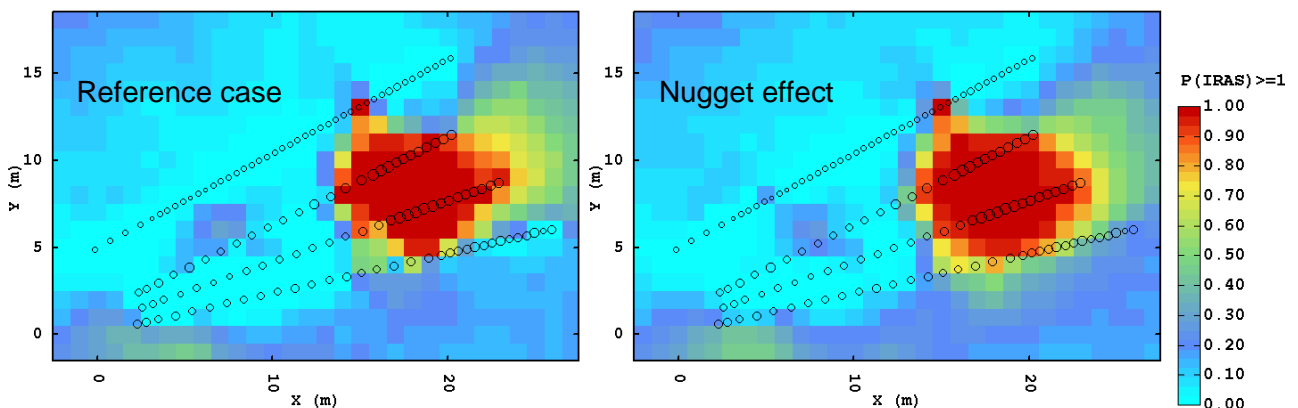


**Figure 31: Comparison of probability that  $IRAS \geq 1$  for the reference case (left) and with a nugget effect (right).**

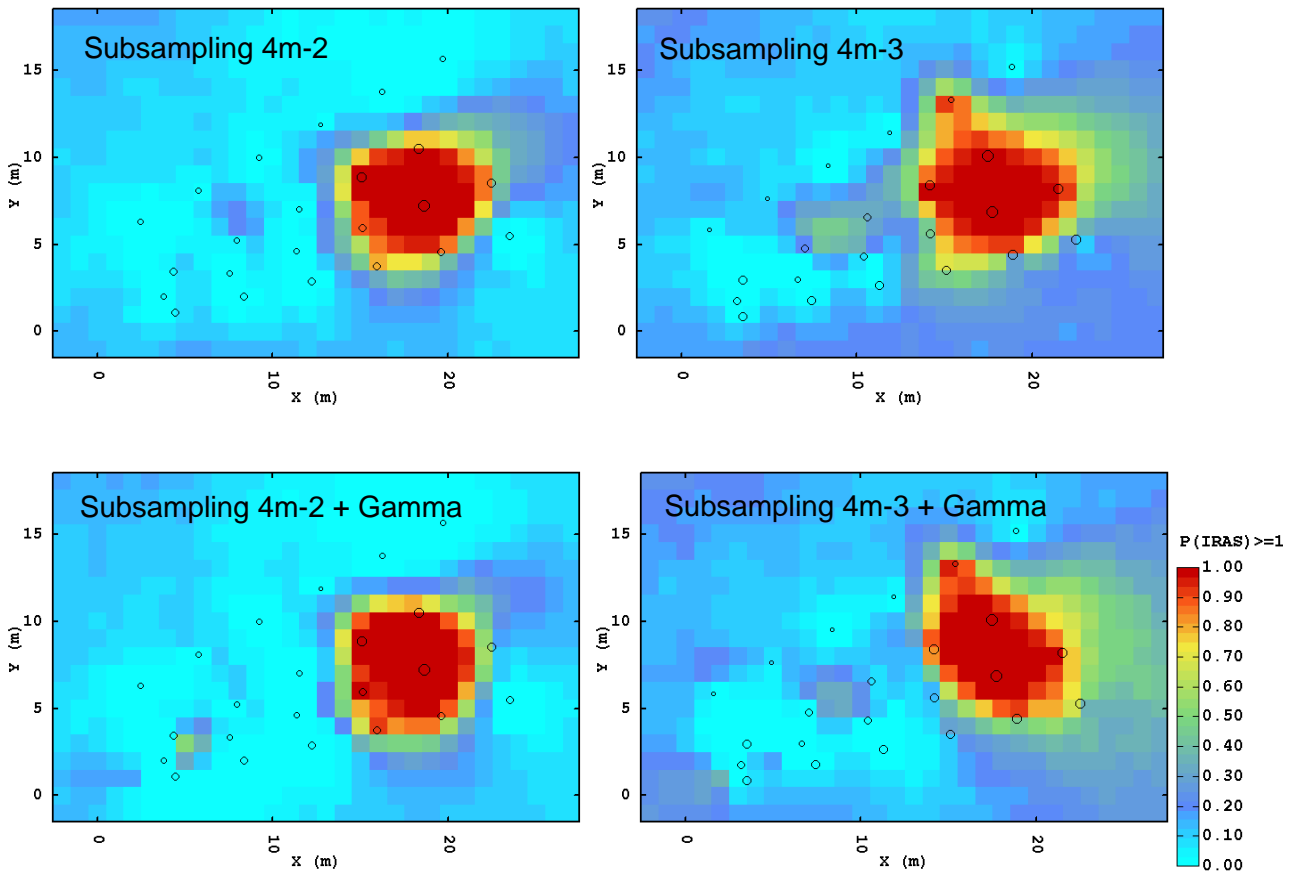


**Figure 32: Comparison of probability that  $IRAS \geq 1$  for 2 possible 4m-subsampling using Gamma scanning or not.**

### 1.2.3.5 Sensitivity to systematic bias around IRAS 1 threshold

Figure 33 summarizes the relative evolution of remediation volumes when the activity concentration levels are biased. For easy calculation, variations are made directly on the IRAS criterion in order to reproduce systematic bias on laboratory results (calibration factor for instance) with factors ranging from 10 to 1/10. For very small resulting fictive IRAS (measurement values are multiplied by a factor 5 or 10), almost all the volume should be remediated, as the fake detection limits are now close to the IRAS 1. In the intermediate range ( $\pm 50\%$  on activity values), volume estimates are quite robust as the slope is lower than the first bisector line. For example, with the quantile 30%:

- -50% underestimation of activity concentration results in a -11% and -22% on volumes for levels H1 (-0,5m) and H2 (-1,5m) respectively,
- +50% overestimation of activity concentration results in a +13% and +26% on volumes similarly.

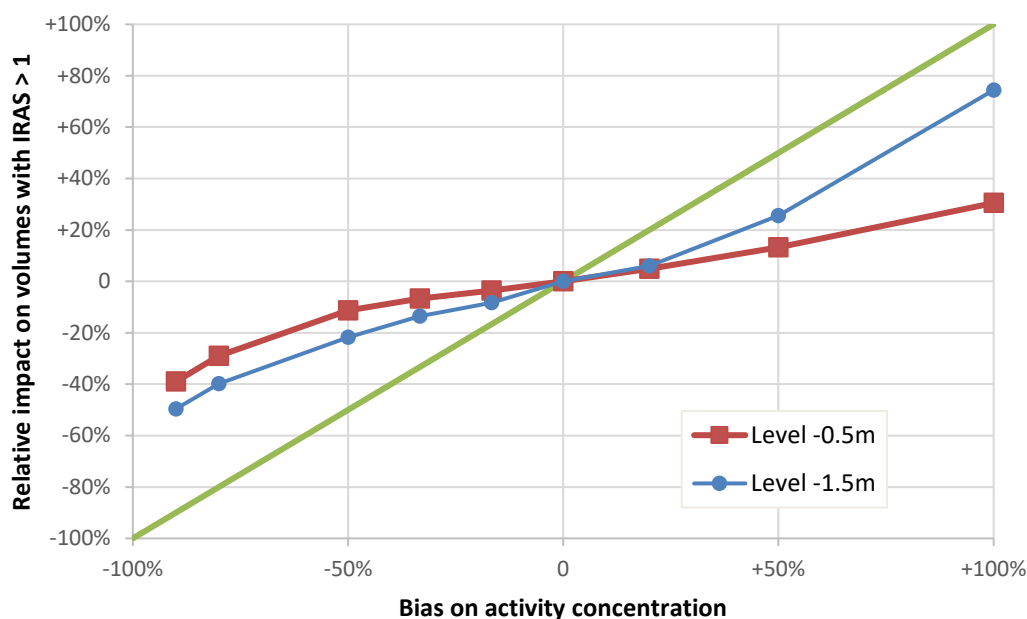


**Figure 33: Evolution of remediation volumes depending on the IRAS threshold for the Reference Case and considering quantile 30%. First bisector line in green.**

## 1.2.4 Post-processing with limits of detection and measurement uncertainties treatment

### 1.2.4.1 Outcomes: Total activity (source term or radiological inventory)

The objectives of the methodologies described in §1.2.2.3 are to provide realistic estimation of the radiological contamination taking into account specific information as limits of detection (called LOD and corresponding here to the decision threshold LD/2 where LD is the detection limit measurement) and measurement uncertainties as incomplete information that are called censored data. The intention here is to show that for some difficult cases with many values below the limit of detection and uncertainty measurements, the benefit to perform specific methodologies can be important. Therefore, the outcomes presented in the next sections for geostatistic method may differ slightly from the previous ones because of the hypothesis (gaussian anamorphosis not performed here, variogram model not fitted with the same method ...) but the important is the compare results obtained with the three methods with the same hypothesis in the next sections.

Both geostatistical methods (*Geo* and *Geo+LOD+U*) provide spatial models for a good estimation of mean<sup>1</sup> and median value of activity by kriging interpolation while the objective of the probabilistic model (*PM+LOD+U*) is to supply a model with a good balance of performances for median and high quantiles.

On Table 5, robustness for the three methods have been assessed and in particular, the predictivity coefficient<sup>2</sup>  $Q^2$  have been estimated for both geostatistical approaches while theoretical and empirical quantiles have been compared for the probabilistic model.

For geostatistical approaches, results are slightly similar with a small difference for the benefit of *GEO+LOD+U* method except for nuclide A at level H2 (-1.5m). For *PM+LOD+U* method, the results show an overestimation of median for nuclide B at level -0.5m, nuclides A and C at level -1.5m. An underestimate of 95% quantile is observed for nuclides A and B at level H1 (-0.5m) and nuclide B at level H2 (-1.5m).

<sup>1</sup> Kriging estimation is done on activities with log transformation and then mean is calculated according mean lognormal distribution formulation.

<sup>2</sup>  $Q^2$  corresponds to  $R^2$  coefficient calculated by cross-validation (IOOSS, 2011) (MARREL, IOOSS, VAN DORPE, & VOLKOVA, 2008).

**Table 5: Robustness and indicators of prediction quality for the different methods performed on the three studied radionuclides.**

Methodology		Predictivity coefficient Q <sup>2</sup>		(PM+LOD+U) Proportion of valid data over quantile curve		
		GEO	GEO+LOD+U	50%	90%	95%
Level -0.5m (H1 plan)	Nuclide A	87%	88%	51%	9.7%	6.5%
	Nuclide B	81%	86%	51%	9%	5.5%
	Nuclide C	91%	91%	50%	16%	4%
Level -1.5m (H2 plan)	Nuclide A	84%	80%	41%	9.8%	4%
	Nuclide B	73%	78%	57%	10%	5%
	Nuclide C	87%	92%	44%	12%	4%

The details of the results for nuclide B for which the uncertainties are the most important are presented here. A surface area of 20 meters long and 30 meters wide is considered. The estimations on each plan have been done for a depth of 1 meter. To have a reference, as illustrated on Figure 34, considering a single hot spot, median activity has been estimated on each ring with a width of 1 meter around the hot spot. The sum of these estimations can be carefully considered as a conservative reference of the total activity and will be called empirical median estimation in the rest of the document.

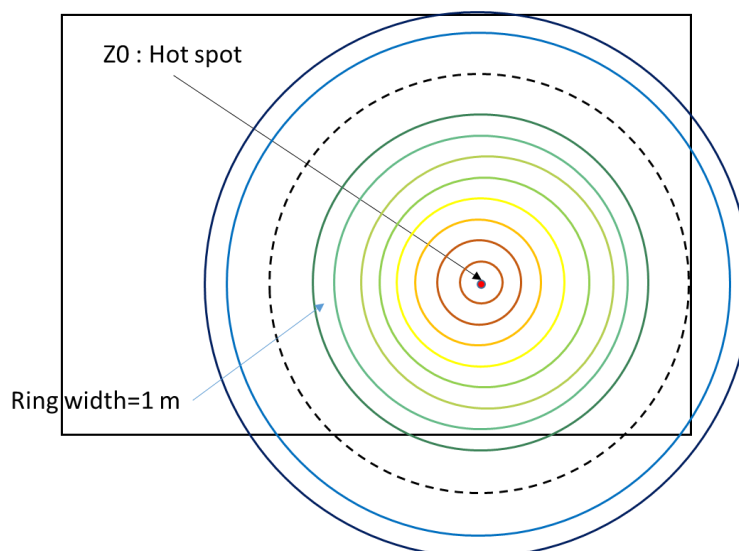


**Figure 34: Strategy to calculate an empirical median estimation of total activity.**

**Table 6: Mean and median estimation of total activity with the empirical approach (circles).**

Total activity (GBq)		Mean	Median
H1 (-0.5m)	A	0.44	0.19
	B	3.48	2.3
	C	1.05	0.24
H2 (-1.5m)	A	0.19	0.15
	B	5.96	2.16
	C	0.73	0.36

Figure 35 shows fitted spherical model variograms of nuclide B at level -0.5m (H1) for both geostatistical methods without any nugget effect. It can be observed that ranges are quite the same, but sills are slightly different, for Geo method sill is higher (17.4 for Geo method and 16.1 for Geo+LOD+U method).

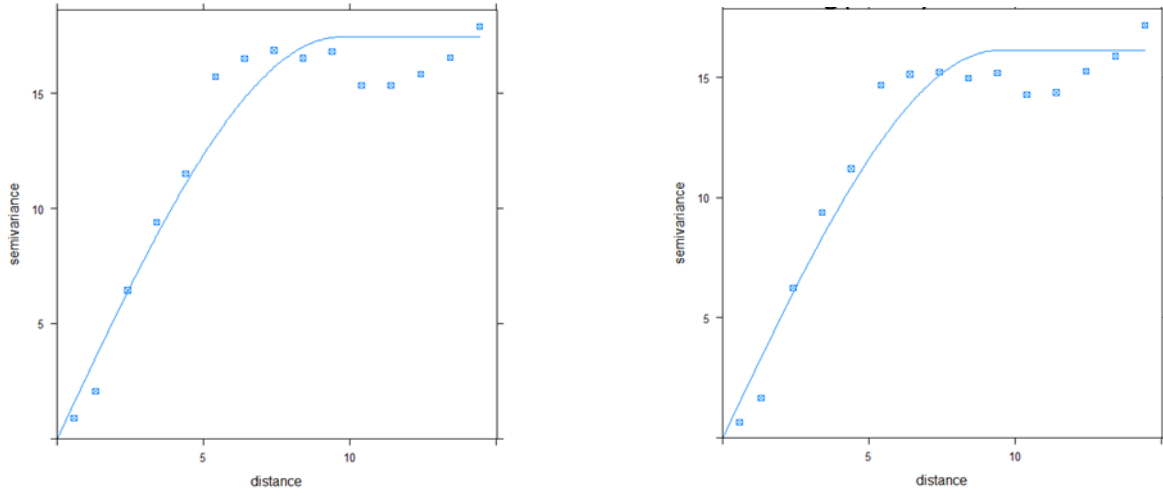


**Figure 35: Spherical model variogram fitted for Geo method on left (a) and for Geo+LOD+U method on right (b) for log(Activity) of nuclide B at level -0.5m (H1).**

Leave-one-out cross validation (LOOCV) visits a data point, and predicts the value at that location by leaving out the observed value, and proceeds with the next data point. (The observed value is left out because kriging would otherwise predict the value itself.) Standardized residuals (SAPORTA, 2006) are the differences between the measurement data and their predictions by LOOCV. Zscore value is the residual divided by kriging standard error.

On Figure 36, representations of zscore values relatively to LOOCV predictions at location of observed values do not show a specific pattern, residuals are distributed on a slightly larger range for Geo method but for both geostatistical methods range of standardized residuals are well distributed on the interval [-2 ;2]. On Figure 36, cross validation scatter plots for Geo and Geo+LOD+U methods are represented to visualize predictions (from LOOCV modeling) versus measurement data. The second graph shows that for Geo+LOD+U method, points are located closer to the axe corresponding to a better predictivity of this geostatistical model.

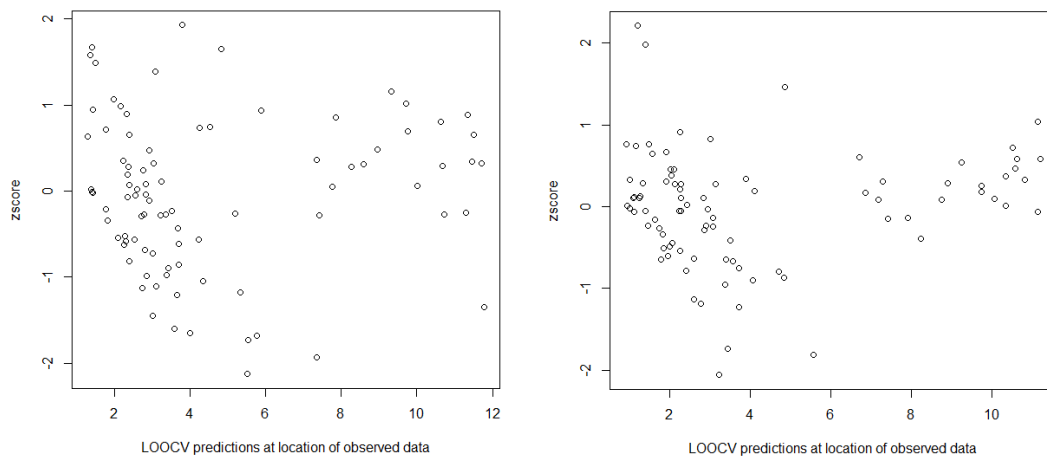


**Figure 36: Residual analysis representation for Geo method on left (a) and for Geo+LOD+U method on right (b) for log(Activity) of nuclide B at level -0.5m (H1).**

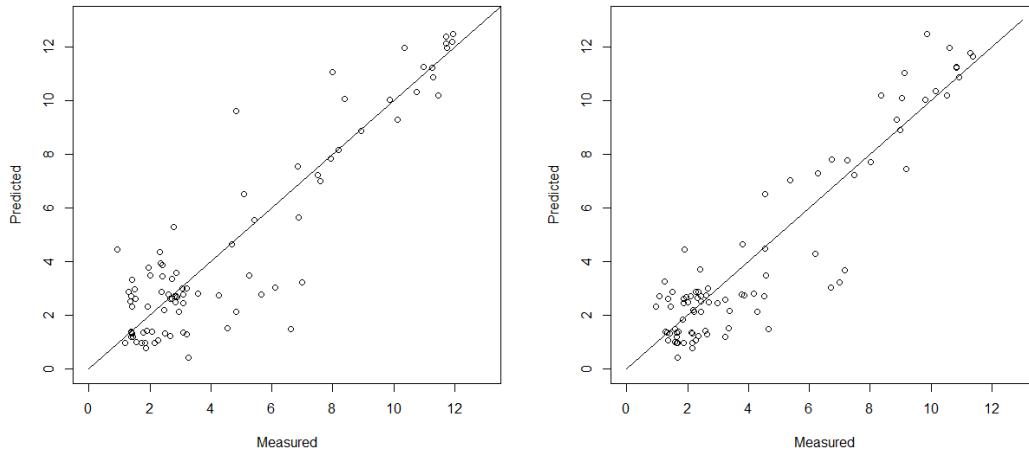


**Figure 37: Cross validation scatter plot for Geo method on left (a) and Geo+LOD+U method on right (b) on lognormal transformation of nuclide B activity at level -0.5m (H1).**

On Figure 45 (a), are presented estimation cartography of  $\log(\text{activity})$  for nuclide B provided with Geo method and on Figure 45 (b) estimations provided by Geo+LOD+U method for H2 plan that show significant differences. These differences are more evident on Figure 46 where the more important variations are localize around the hot spot.

On Figure 38 (a), are presented estimation cartography of  $\log(\text{activity})$  for nuclide B provided with Geo method and on Figure 38 (b) estimations provided by Geo+LOD+U method for H1 plan that show some differences that are more evident on Figure 39. The most important variations are localize around the hot spot.

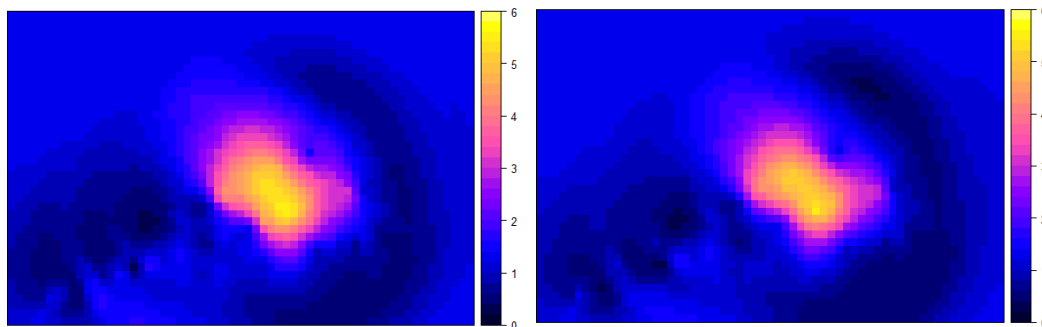


**Figure 38: Estimation cartography of  $\log_{10}(\text{activity})$  for nuclide B provided with ordinary kriging on data without uncertainty and specific treatment for limits of detection (Geo) on the left (a), with uncertainty and specific treatment for limits of detection with Geo+LOD+U method in the middle (b) at level -0.5m (H1).**

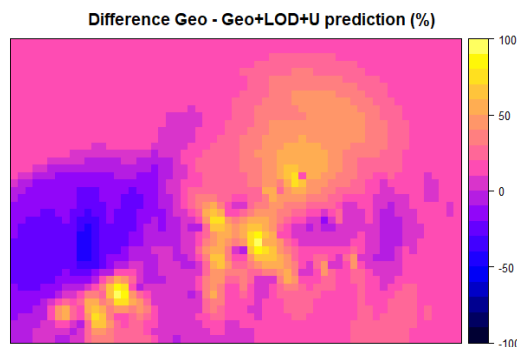


**Figure 39: Cartography representation of difference between Geo ordinary kriging predictions and GEO+LOD+U ordinary kriging predictions for activity of nuclide B at level -0.5m (H1).**

The graphs of kriging variance represented on Figure 40 show that the geostatistical models give more accurate predictions for the points inside the convex hull of data measurements and that variance values are slightly higher for Geo method.

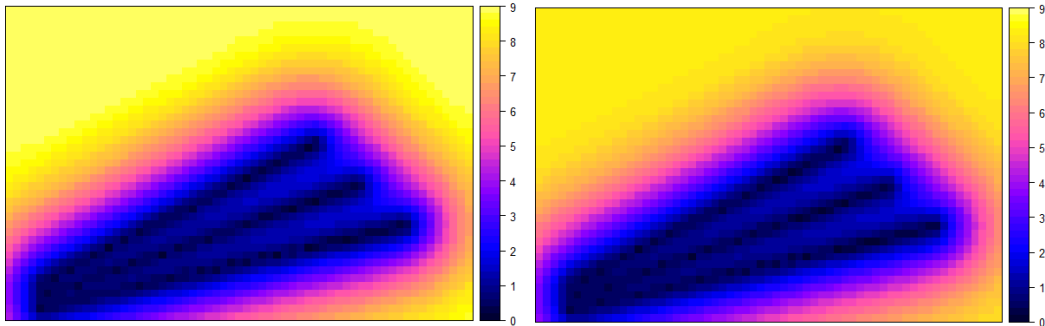


**Figure 40: Kriging variance for Geo method on left (a) and for Geo+LOD+U method on right (b) for  $\log_{10}(\text{nuclide B})$  at level -0.5m (H1).**

For each radionuclide and each level, the location of the hot spot has been identified and for the third method (*PM+LOD+U*), a lognormal distribution have been fitted with parameters that are functions of the distance  $\rho$  from the hot spot. For  $\log_{10}(\text{Activity})$  of nuclide B on Figure 41 (a) and Figure 48 (a), the quantile curves show a better fitting of the probabilistic model for high nuclide B activities and an overestimation for lower activities at level -0.5m (H1). This is due to the fact that with this method, the fitting is done on valid data and corrected by censored data (LOD and uncertainty measurements) and this correction can be limited when the number of values below the LOD is very important. Then estimations can be conservative for high quantiles.

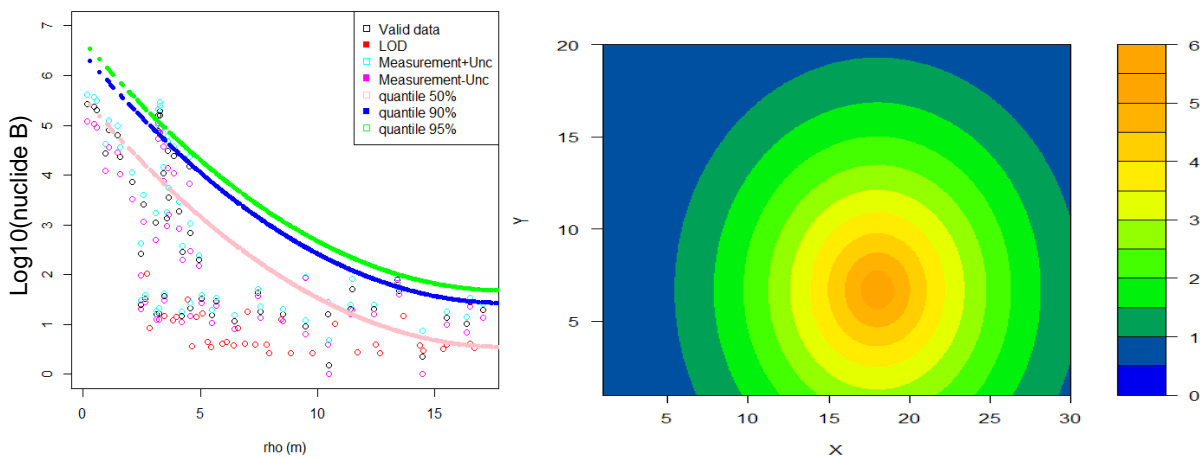


**Figure 41: Quantile curve estimations and median estimation cartography of  $\log_{10}(\text{activity})$  for nuclide B provided with *PM+LOD+U* method at level H1 (-0.5m).**

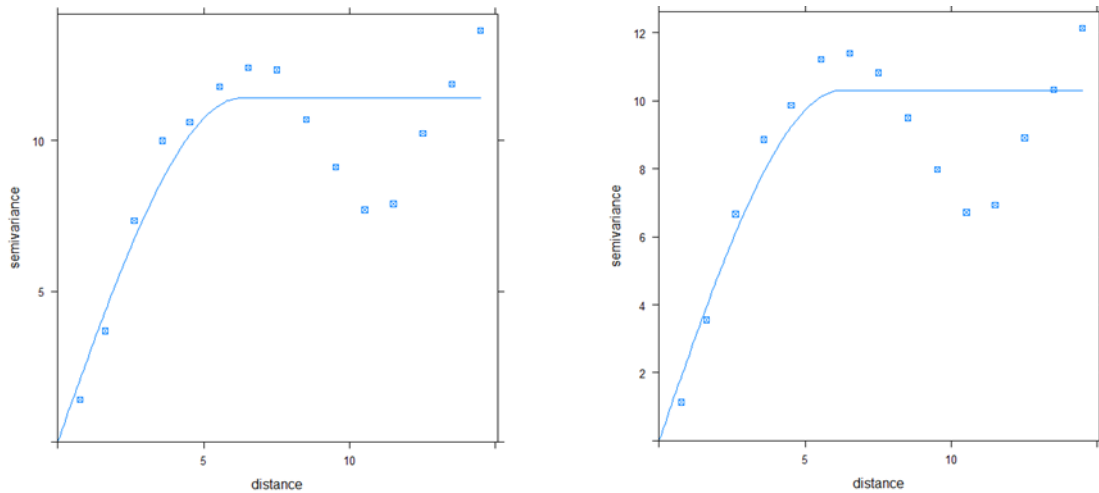


**Figure 42: Spherical model variogram fitted for Geo method on left (a) and for Geo+LOD+U method on right (b) for nuclide B at level H2 (-1.5m).**

On Figure 43, representations of zscore values relatively to LOOCV predictions at location of observed values do not show a specific pattern, the majority of the residuals are distributed on the interval [-2 ;2]. On Figure 44, cross validation scatter plots for Geo and Geo+LOD+U methods are represented to visualize predictions (from LOOCV modeling) versus measurement data. The second graph shows that for Geo+LOD+U method, points are located closer to the axe corresponding to a better predictivity of this geostatistical model.

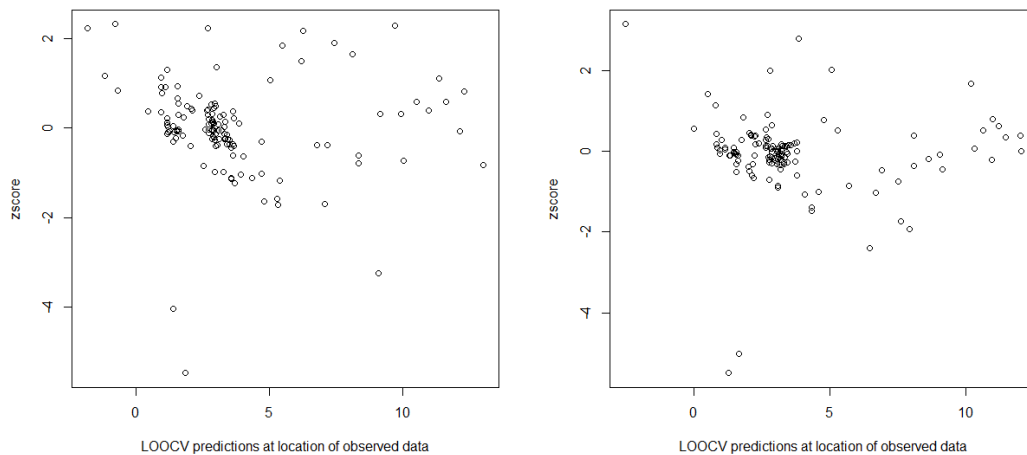


**Figure 43: Residual analysis representation for Geo method on left (a) and for Geo+LOD+U method on right (b) for log(nuclide B) at level H2 (-1.5m).**

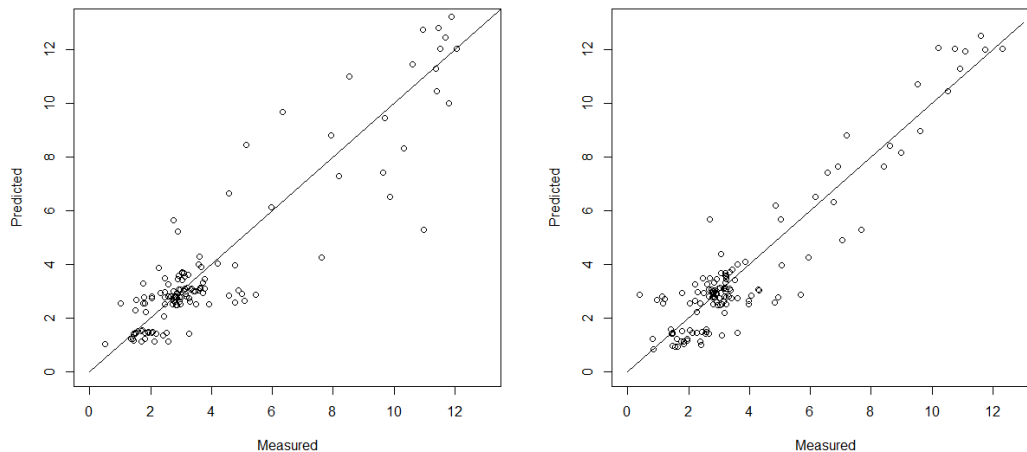


**Figure 44: Cross validation scatter plot for Geo method on left (a) and Geo+LOD+U method on right (b) on lognormal transformation of nuclide B activity at level H2 (-1.5m).**

On Figure 45 (a), are presented estimation cartography of  $\log(\text{activity})$  for nuclide B provided with Geo method and on Figure 45 (b) estimations provided by Geo+LOD+U method for H2 plan that show significant differences. These differences are more evident on Figure 46 where the most important variations are localize around the hot spot.

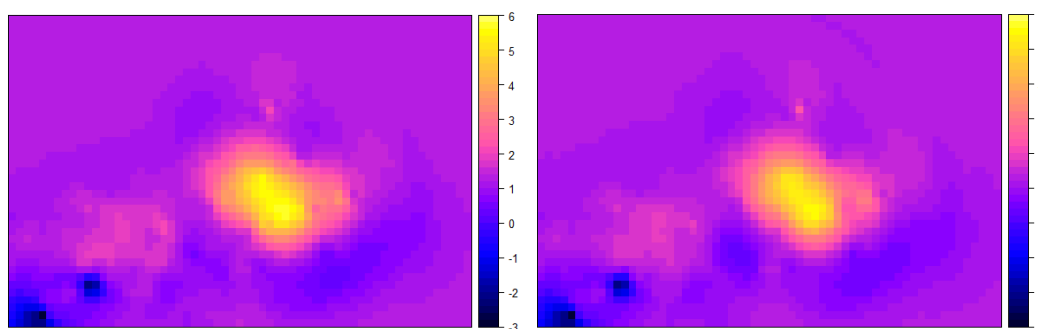


**Figure 45: Estimation cartography of  $\log_{10}(\text{activity})$  for nuclide B provided with ordinary kriging on data without uncertainty and specific treatment for limits of detection *with* Geo on left (a) and with uncertainty and specific treatment for limits of detection with Geo+LOD+U method on right (b) at level H2 (-1.5m).**

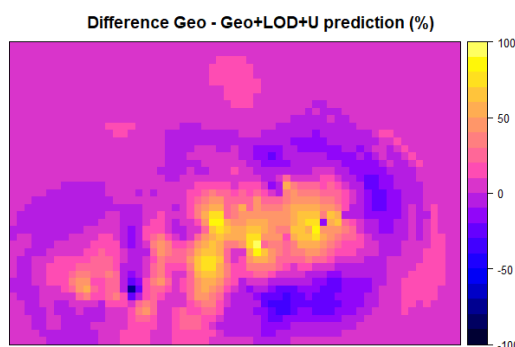


**Figure 46: Cartography representation of difference between Geo ordinary kriging predictions and GEO+LOD+U ordinary kriging predictions for activity of nuclide B at level H2 (-1.5m).**

The graphs of kriging variance represented on Figure 47 show that the geostatistical models give more accurate predictions for the points inside the convex hull of data measurements and that variance values are slightly higher for Geo method.

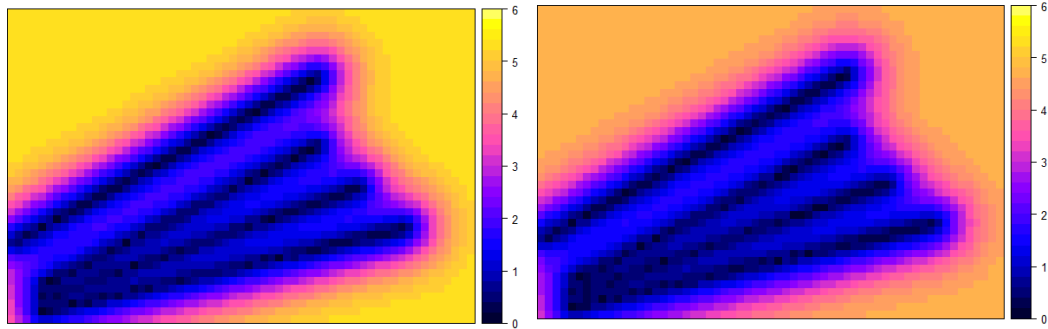


**Figure 47: Kriging variance for Geo method on left (a) and for Geo+LOD+U method on right (b) for  $\log_{10}(\text{nuclide B})$  at level H2 (-1.5m).**

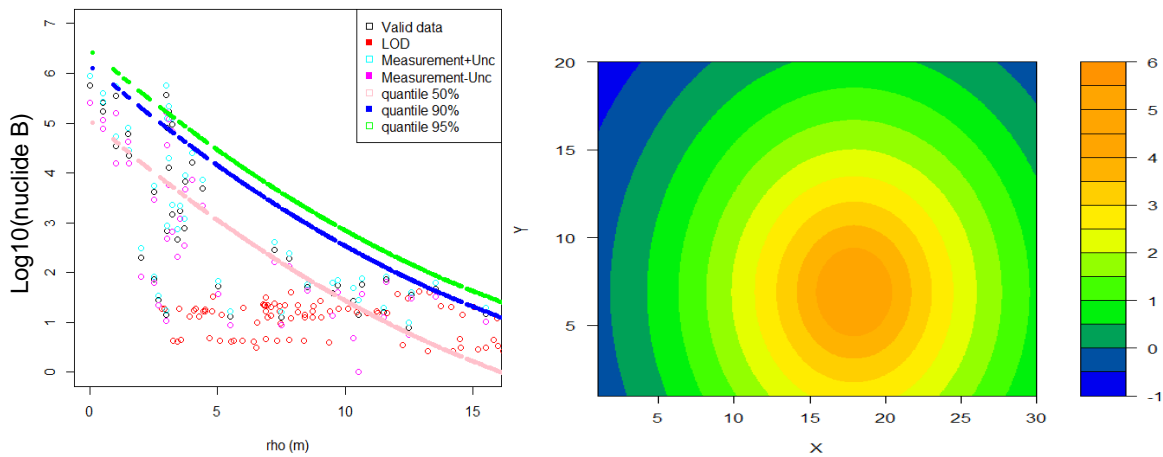


**Figure 48: Quantile curve estimations and median estimation cartography of  $\log(\text{activity})$  for  $\log_{10}(\text{Nuclide B})$  provided with PM+LOD+U method at level H2 (-1.5m).**

To estimate quantiles for both geostatistical methods and the three studied radionuclides, geostatistical conditional simulations (200 simulations) have been performed on the convex hull of data measurements and a depth of 1 meter. For PM+LOD+U method, quantiles have been estimated on the complete domain area of 20 meters long and 30 meters wide and a depth of 1 meter for each level. The corresponding areas with observation locations are presented on Figure 49.

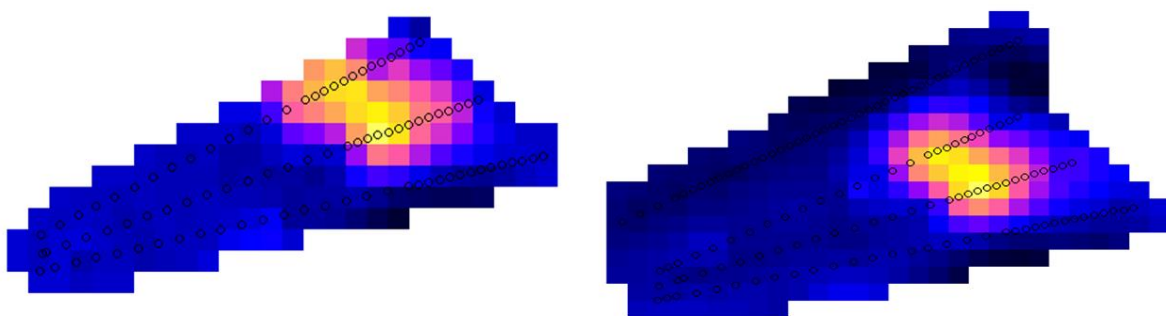
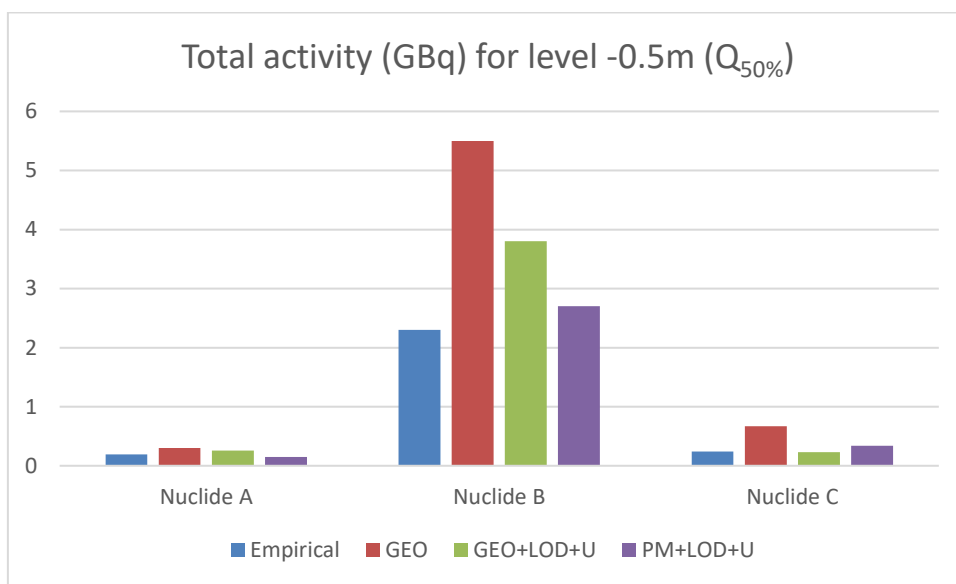


**Figure 49: Convex hull of data measurements used for geostatistical simulations at level H1 (-0.5m) on left and level H2 (-1.5m) on right.**

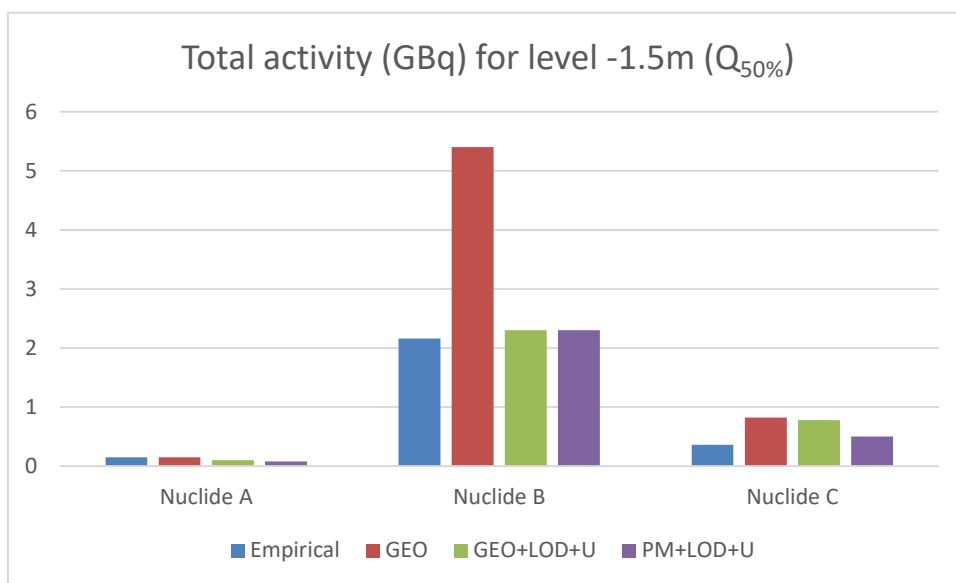
On Table 7, quantile estimations of total activity for the three methods show significant differences between methods taking into account limits of detection and uncertainties and the method that do not. Compared to empirical estimation (Table 6), which is not the real value but a conservative reference, not taking into account limits of detection and uncertainty penalized the estimations. Bar charts of Figure 50 and Figure 51 illustrate these results for level H1 (-0.5m) and level H2 (-1.5m).

**Table 7: Median and 5% and 95% quantile estimates of total activity for the three studied radionuclides and both levels.**

Total activity (GBq)		Estimation Q <sub>50%</sub>				Interval [Q <sub>5%</sub> ; Q <sub>95%</sub> ]		
Methodology		Empirical	GEO	GEO+LOD+U	PM+LOD+U	GEO	GEO+LOD+U	PM+LOD+U
H1 (-0.5m)	A	0.19	0.3	0.26	0.15	[0.15 ; 1.1]	[0.12 ; 0.9]	[0.04 ; 615]
	B	2.3	5.5	3.8	2.7	[2.3 ; 18.4]	[1.6 ; 13.2]	[0.2 ; 37]
	C	0.24	0.67	0.23	0.34	[0.3 ; 2.4]	[0.12 ; 0.64]	[0.01 ; 11.3]
H2 (-1.5m)	A	0.15	0.15	0.1	0.08	[0.06 ; 0.5]	[0.04 ; 0.3]	[0.002 ; 2.8]
	B	2.16	5.4	2.3	2.3	[2.7 ; 17.9]	[1.2 ; 6.1]	[0.1 ; 31.3]
	C	0.36	0.82	0.78	0.5	[0.4 ; 2.14]	[0.4 ; 2.4]	[0.01 ; 14.4]

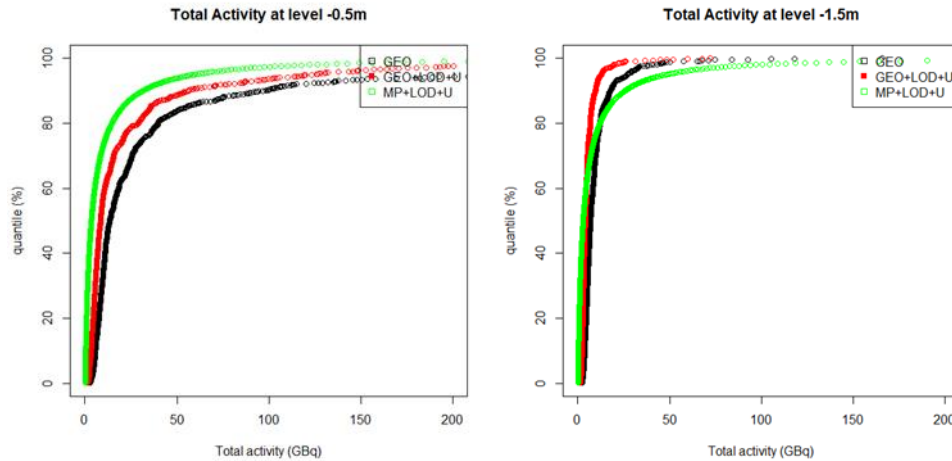


**Figure 50: Median estimations from simulations the three nuclide total activity for the three methods and empirical estimation for H1 plan (level H1 at -0.5 m).**



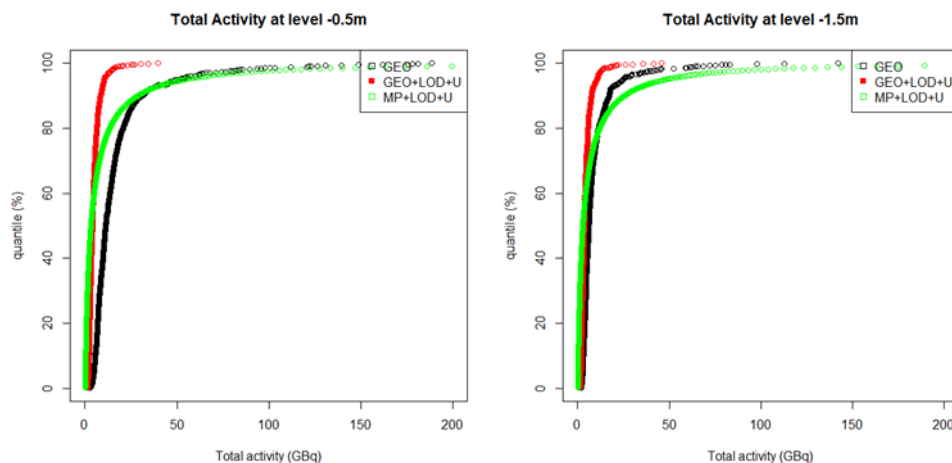
**Figure 51: Median estimations from simulations of the three nuclide total activity for the three methods and empirical estimation for H2 plan (level H2 at -1.5 m).**

Figure 52 (a) shows that for H1 plan, quantile estimations of total activity for the total domain area (20 meters long and 30 meters wide and a depth of 1 meter for each level) give lower values for *Geo+LOD+U* and *PM+LOD+U* methods than for *Geo* method. On Figure 52 (b), for H2 plan, quantile estimations of total activity are slightly lower for *Geo+LOD+U* on high quantiles. *PM+LOD+U* method in this case gives estimations more conservative for high quantiles and slightly lower for low quantiles.



**Figure 52: Quantile estimations of total activity for the three methods for H1 plan (level -0.5 m) on left (a) and H2 plan (level -1.5 m) on right (b).**

Figure 53 (a) illustrates that for H1 plan, high quantile estimations of total activity for the convex hull of data measurements give lower values for *Geo+LOD+U* and *Geo* methods than for *PM+LOD+U* method but for quantiles lower than 80% outcomes for *Geo+LOD+U* and *PM+LOD+U* are lower. On Figure 53 (b), for H2 plan, the same outcomes are observed for high quantiles, but for quantiles lower than 80% the results are slightly comparable.



**Figure 53: Quantile estimations of total activity on the convex hull of data measurements for the three methods for H1 plan (level -0.5 m) on left (a) and H2 plan (level -1.5 m) on right (b).**

#### 1.2.4.2 Study on IRAS threshold

As presented in §1.2.3.4, the IRAS threshold is used to identify the remediation volume that can be classified as Very-Low Level waste and defined by:

$$\frac{\text{Nuclide A}}{10} + \frac{\text{Nuclide B}}{1000} + \frac{\text{Nuclide C}}{10} \geq 1$$

IRAS calculations were performed with simulations on the total domain area (20 meters long and 30 meters wide and a depth of 1 meter for each level). On Figure 54, the curves for the quantiles of

probability to exceed the IRAS threshold for the three methods show that for low risk, Geo+LOD+U method and PM+LOD+U method are less severe at -0,5m (H1). For H2 level (-1,5m), results for Geo and Geo+LOD+U are very similar and for very low risk, PM+LOD+U method gives lower results.

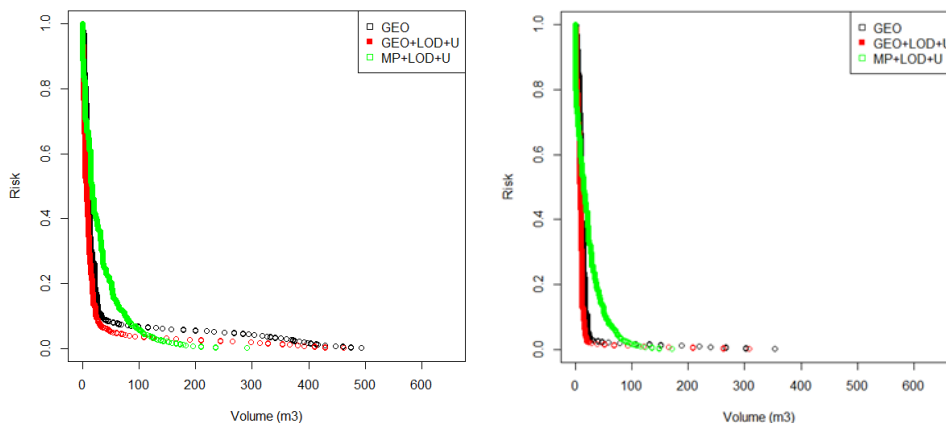


**Figure 54: Risk of exceeding the IRAS threshold for the three methods on the total domain area at level -0.5m (H1) and level -1.5m (H2).**

IRAS calculations were also performed with simulations on the convex hull of data locations. On Figure 55, the curves for the quantiles of probability to exceed the IRAS threshold for the three methods show that for low risk, results for Geo and Geo+LOD+U methods are close and PM+LOD+U method is more severe at -0,5m (H1). For H2 level (-1,5m), results for Geo and Geo+LOD+U are very similar and for very low risk, PM+LOD+U method gives greater results but less severe than for H1 plan.

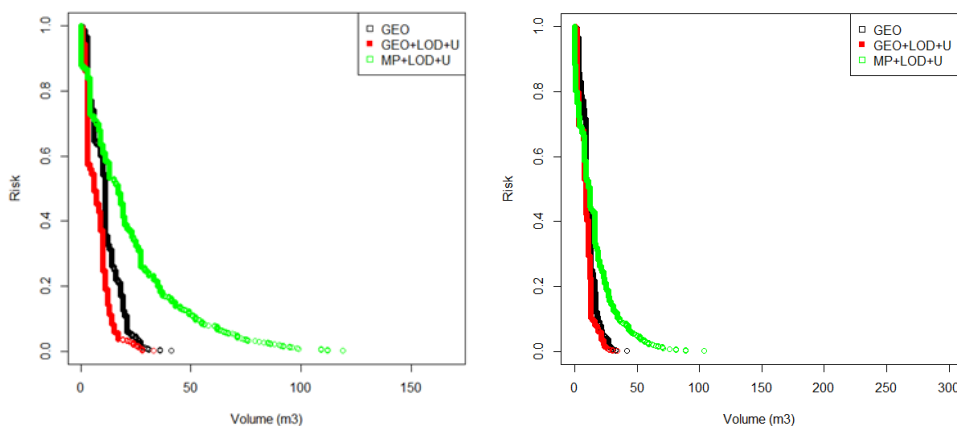


**Figure 55: Risk of exceeding the IRAS threshold for the three methods on the convex hull of data locations at level -0.5m (H1) and level -1.5m (H2).**

### 1.3 Is the objective achieved?

#### 1.3.1 Estimate and uncertainty impact synthesis

Table 8 sums up the main results as regards impact of the different variants to the total activity on the one hand and volumes with an IRAS exceeding 1 on the other hand. As expected, outcomes prove to be quite consistent and robust as expected:

- Nugget effect has limited impact even if estimates are naturally attracted to the mean (which leads to little underestimation of total activity in particular).
- 3D modelling significantly improves results for level H1 (-0,5m) as the extra borehole at lower level -1.5m reduces extrapolation area above.



- Sampling reduction deteriorate almost all results: the less the data, the more the uncertainties.
- Integration of gamma scanning improve almost all results: the more the data (even if comes from in-situ and relative measurements), the less the uncertainties.
- Integration of limits of detection and measurement uncertainty seems to provide lower values for total activity estimations. Nevertheless, in this case, for estimations of exceeding IRAS threshold, the benefit of taking into account limits of detection and uncertainties is not important.

**Table 8: Sensitivity analysis on results (both estimate and related uncertainty).**

Level	Quantity	Estimate	+15% nugget effect	3D modeling	Sampling reduction	Multi-variate ( $\gamma$ scan.)	Geo+ LOD+U	PM+ LOD+U
		Uncertainty						
H1 -0.5m	Total activity	Q50	↘	↓	↗	↘	↘	↘
		Q95-Q5	↗	↓	↗	↘	↘	↑
	IRAS > 1	Q30	↗	↓	↗	↘	↘	↑
		Q10-Q50	↘	↘	↘	↗	↘	↑
H2 -1.5m	Total activity	Q50	↘	→	↘	→	↘	↘
		Q95-Q5	↘	↘	↗	↘	↘	↑
	IRAS > 1	Q30	↗	→	→	→	→	→
		Q10-Q50	→	→	↗	→	→	↑

↑	↗	→	↘	↓
Significant increase (> +50 %)	Slight increase (> +10 %)	Quite comparable (between ±10 %)	Slight decrease (> -10 %)	Significant decrease (> -50 %)

Another issue is the impact of systematic bias on final results in the geostatistical framework. If an affine transformation  $a.X + b$  is used on lab result and similarly  $c.Y + d$  on in situ measurement, then:

- “c” and “d” have absolutely no impact for source term nor waste classification as they are only related to the auxiliary data.
- “a” will directly acts as multiplicative coefficient on source term and “b” as an additive constant. However for waste classification with threshold far from extreme values (detection limit on the one hand and really elevated values on the other hand), “b” has a negligible impact if it can be considered as negligible in comparison to the threshold, and “a” has a relatively limited impact as seen previously (§1.2.3.5).

### 1.3.2 Overall conclusions and sampling recommendations

The statistics and geostatistics methods used in the application case are able to provide several kinds of results such as quantiles of total activity on the one hand and classification of contaminated materials according to the risk to exceed a given threshold (such as French IRAS requirement) on the other hand. These outputs are key results to develop, manage and optimize D&D scenarios. In

addition, it can be relevant to take into account limits of detection and measurement uncertainty to refine the calculations.

Geostatistics proves to be very effective for the analysis of collected data and in order to provide estimates of contaminated materials for different radiological thresholds or total radiological inventory. But there is not a defined standard or guide to define number of measures/boreholes/samples and their location as it strongly depends on the spatial structure of the contamination. Similarly, sampling resolution along drilling cores may benefit from gamma-scanning prior to the sampling step to reduce laboratory analyses.

That way, sampling optimization for the characterization of soils may significantly benefits from a better integrated process, considering a combination of sampling design between in situ measurements and destructive samples thanks to a geostatistics data processing to improve estimates and reduce uncertainties.

Generally speaking, placing drilling points throughout the area is relevant to avoid extrapolation, i.e. estimating the main variable with too high uncertainty, even if there is a good coverage of the auxiliary variable (dose rate, count rate, gamma scanning...). Focusing only on certain (contaminated) areas overfits the statistical distribution to certain (high) values, thus result in biasing the calculation if not considered adequately and neglecting areas with lower activity levels. On the other hand, it is necessary to sample the supposedly least contaminated zones as well as the most contaminated zones to achieve a realistic understanding of the statistical distribution of the contamination (important for normal score transformation and correlation with indirect measurement).

Similarly, the spatial distribution of in-depth investigations shall cover the entire site to characterize it globally. Confirming some contamination-free areas is often as important as (or even more important than) confirming some other areas as contaminated, already known from the site history. However, from the point of view of waste volume management, transition zones are more critical since it is difficult to categorize them with respect to the reference thresholds (intermediate probability levels ranging from 10% to 50% as used in this use case). Uncertainty being the most important in these areas for proper delineation (and limiting misclassification errors), the sampling distribution should favour them over other areas that only require confirmation of contamination or non-contamination.

So, as a general statement and conclusion, sampling strategy is strongly affected by the characterization objectives, the historical context and also needs the quantification of the related uncertainties on final results that results from the data processing technique and model hypotheses.